

Human 3D cellular model of hypoxic brain injury of prematurity

Anca M. Paşca¹, Jin-Young Park², Hyun-Woo Shin^{1,2,3}, Qihao Qi⁴, Omer Revah^{1,2}, Rebecca Krasnoff⁴, Ruth O'Hara², A. Jeremy Willsey⁴, Theo D. Palmer⁵ and Sergiu P. Paşca^{1,2*}

Owing to recent medical and technological advances in neonatal care, infants born extremely premature have increased survival rates^{1,2}. After birth, these infants are at high risk of hypoxic episodes because of lung immaturity, hypotension and lack of cerebral-flow regulation, and can develop a severe condition called encephalopathy of prematurity³. Over 80% of infants born before post-conception week 25 have moderate-to-severe long-term neurodevelopmental impairments⁴. The susceptible cell types in the cerebral cortex and the molecular mechanisms underlying associated gray-matter defects in premature infants remain unknown. Here we used human three-dimensional brain-region-specific organoids to study the effect of oxygen deprivation on corticogenesis. We identified specific defects in intermediate progenitors, a cortical cell type associated with the expansion of the human cerebral cortex, and showed that these are related to the unfolded protein response and changes. Moreover, we verified these findings in human primary cortical tissue and demonstrated that a small-molecule modulator of the unfolded protein response pathway can prevent the reduction in intermediate progenitors following hypoxia. We anticipate that this human cellular platform will be valuable for studying the environmental and genetic factors underlying injury in the developing human brain.

Extremely premature birth (before post-conception week (PCW) 28) coincides with critical biological events in the development of the central nervous system, including the formation of the expanded human cerebral cortex. Encephalopathy of prematurity is characterized by gray- and white-matter abnormalities and a reduction in cortical volume that correlates with neurodevelopmental outcomes, including cognitive and behavioral disorders¹. A common pathogenic factor in encephalopathy of prematurity appears to be perinatal hypoxia⁵ (often considered as decreases in the partial pressure of oxygen (P_{O_2}) below 40 mmHg). However, the cellular substrates and the molecular mechanisms by which changes in oxygen tension lead to cortical gray-matter defects in extremely premature infants are still not understood. This is primarily due to challenges in directly investigating the preterm human brain and difficulties in recapitulating the trajectory of human brain development and maturation in other species. Moreover, the unique cellular and molecular features underlying cortical development in humans⁶ underscore the need for personalized human models of brain development. Recent advances in cell-reprogramming technologies as well as three-dimensional (3D) cell-differentiation methods make

possible the non-invasive derivation of structures resembling regions of the developing human brain⁷.

Here we leveraged a method that we have previously described^{8–10} to develop an in vitro human cellular model of hypoxic encephalopathy of prematurity. To achieve this, we differentiated human induced pluripotent stem (hiPS) cells into brain-region-specific organoids called human cortical spheroids (hCS)^{9–11}. After approximately 10 weeks in vitro, hCS transcriptionally resemble the cerebral cortex at midgestation^{9,10}, which approximately corresponds to extreme prematurity. This developmental stage is characterized by extensive proliferation and neurogenesis in the cerebral cortex—a process that continues into the third trimester of pregnancy^{12–14}. We exposed hCS to low oxygen concentrations in vitro and found a reduction in a specific population of cortical progenitors that are thought to contribute to the expansion of the primate cerebral cortex. Moreover, we found that pharmacologically modulating the unfolded protein response (UPR) can prevent this defect, and we used human primary tissue to validate these findings.

To develop a model of hypoxia during human corticogenesis, we differentiated hCS from five hiPS cell lines derived from four healthy subjects (Fig. 1a and Supplementary Table 1). We used a gas control chamber to expose hCS at approximately day 75 of differentiation to low oxygen tension (<1%) for 48 h, followed by reintroduction to 21% O_2 . To monitor changes in P_{O_2} in hCS, we used a needle-type fiber-optic oxygen microsensor. At the surface of hCS, the P_{O_2} was approximately 85 mmHg, which is similar to P_{O_2} in arterial blood, while in the center values were on average above 62 mmHg (Fig. 1b and Extended Data Fig. 1a). Exposure to <1% O_2 for 48 h resulted in a drop to approximately 25 mmHg at the hCS surface and approximately 20 mmHg in the center of hCS, which is below the critical oxygen tension in the brain ($P < 0.0001$)¹⁵. Whole-hCS western blot analysis demonstrated that hypoxia-inducible factor-1 alpha (HIF-1 α), a key oxygen-labile protein in the hypoxia pathway, stabilized at 48 h in low oxygen ($P = 0.02$) and returned to previous levels following 72 h of reoxygenation (Fig. 1c,d and Supplementary Table 2). Similarly, immunocytochemistry in hCS cryosections indicated the expected nuclear localization of the HIF-1 α protein (Fig. 1e). At the same time, the level of cell death as estimated by cleaved caspase-3 (c-CAS3) did not significantly increase during exposure to <1% O_2 ($P = 0.29$; Extended Data Fig. 1b,c), suggesting that a hypoxia-like response was induced without massive cell death. We next investigated the transcriptional changes associated with exposure to <1% O_2 by performing RNA sequencing at 24 and 48 h (middle and end of <1% O_2 exposure

¹Department of Pediatrics, Division of Neonatology, Stanford University, Stanford, CA, USA. ²Department of Psychiatry and Behavioral Sciences & Stanford Human Brain Organogenesis Program, Stanford University, Stanford, CA, USA. ³Department of Pharmacology and Biomedical Sciences, Seoul National University, Seoul, Republic of Korea. ⁴Institute for Neurodegenerative Diseases and Department of Psychiatry, UCSF Weill Institute for Neurosciences, University of California, San Francisco, CA, USA. ⁵Department of Neurosurgery, Stanford University, Stanford, CA, USA. *e-mail: spasca@stanford.edu

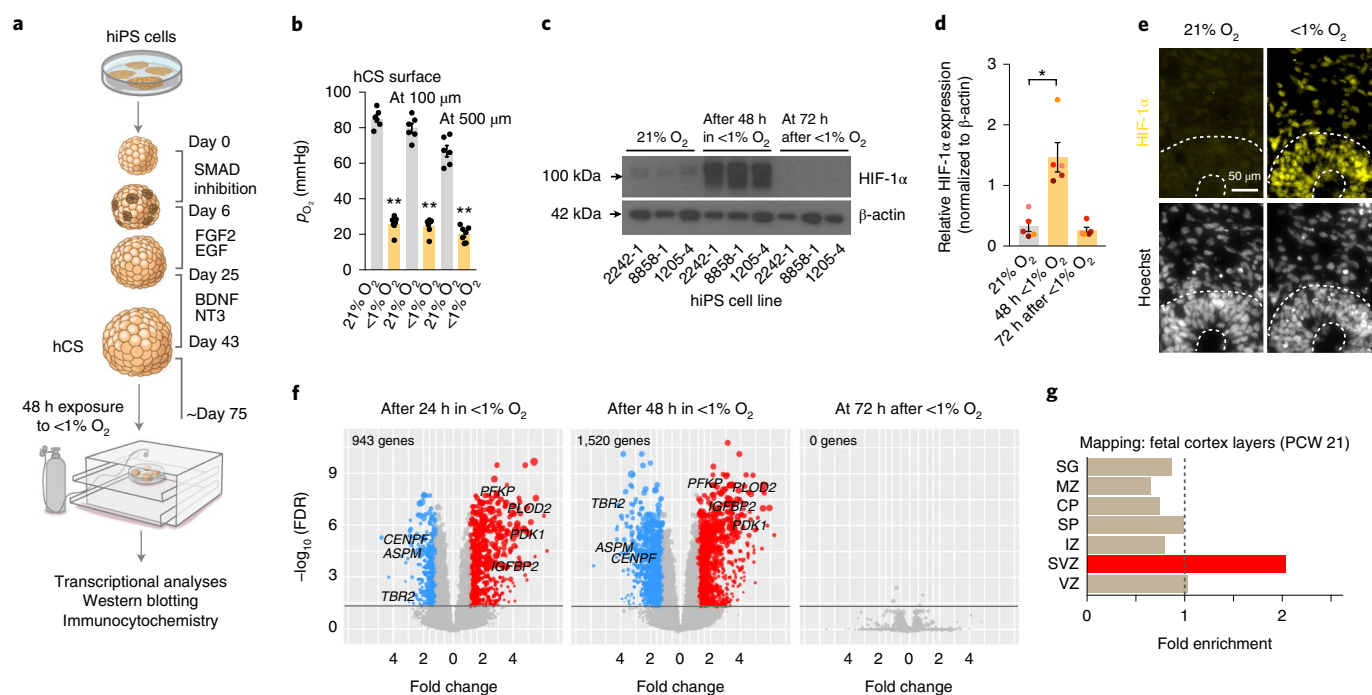


Fig. 1 | Human cellular model for studying changes in oxygen tension in hCS. **a**, Schematic of the major stages in the generation of hCS from hiPS cells as described in ref. ⁹. At days 74–78 of *in vitro* differentiation, hCS are exposed for 48 h to $<1\%$ O_2 in a gas-controlled culture chamber and then maintained for another 72 h at 21% O_2 . Control hCS are maintained at 21% O_2 throughout. **b**, Oxygen tension levels (P_{O_2} , mmHg) measured with an optical sensor (100 and 500 μm) at 21% O_2 ($n=6$ hCS) and after 48 h of exposure to $<1\%$ O_2 ($n=7$); hCS from three hiPS cell lines; Kruskal–Wallis test, $P < 0.0001$, Dunn’s multiple-comparison test, $**P = 0.002$ at hCS surface, $**P = 0.008$ at 100 μm , $**P = 0.01$ at 500 μm . **c,d**, Representative western blots and quantification of HIF-1 α protein expression in hCS after 48 h of exposure to $<1\%$ O_2 and after 72 h of reoxygenation versus the unexposed samples (21% O_2); normalized to β -actin ($n=5$ differentiated hiPS cell lines with at least two hCS per condition; Friedman’s test, $P = 0.02$, Dunn’s multiple-comparison test versus 21% O_2 , $*P = 0.02$ for 48 h and $P > 0.99$ for 72 h). Data are mean \pm s.e.m. Individual values are indicated by dots. Western blots were cropped to show the relevant bands; molecular weight markers are indicated on the left (in kDa). See Supplementary Table 2 for quantifications, and uncropped blots are available as source data. **e**, Representative immunostaining of HIF-1 α (yellow) in hCS exposed for 48 h to $<1\%$ O_2 versus 21% hCS. Experiment performed in two hiPS cell lines. Nuclei labeled by Hoechst staining. **f**, Volcano plots showing the results of RNA-seq experiments after exposure to $<1\%$ O_2 for 24 h or 48 h versus 21% O_2 , as well as after 48 h of exposure to $<1\%$ O_2 followed by 72 h of reoxygenation (total time of 120 h). Each dot represents a single gene, with genes that are significantly upregulated shown in red, genes that are significantly downregulated in blue and non-significant genes in gray (determined on the basis of $FDR \leq 0.05$ and fold change ≥ 1.5). The size of the points corresponds to the difference in expression level between low-oxygen-exposed hCS and unexposed hCS (difference of medians); $n=24$ samples from hCS derived from three hiPS cell lines. **g**, Overlap between hypoxia-related transcriptome changes in hCS and layer-specific transcriptome signatures in the developing human cortex at PCW 21 as described in ref. ¹⁶. Strong enrichment is observed only in SVZ (P value corrected for multiple-comparisons). SG, subplate granular zone; MZ, marginal zone; CP, cortical plate; SP, subplate; IZ, intermediate zone; VZ, ventricular zone.

interval), as well as after 72 h of reoxygenation at 21% O_2 (Fig. 1f). Hierarchical clustering of the gene expression profiles separated the samples exposed to $<1\%$ O_2 from unexposed samples at 24 h and 48 h, but not at 72 h after reoxygenation (time = 120 h). Together, these findings suggest that exposure to low oxygen levels resulted in a defined transcriptional profile, and that after 72 h at atmospheric oxygen, hCS reverted to their expression state before exposure to low oxygen (Extended Data Fig. 2a). To identify genes associated with the response to low oxygen we identified genes differentially expressed between the hCS exposed $<1\%$ O_2 and the hCS exposed to 21% O_2 . We tested and controlled for potential confounding variables, such as genetic background, differentiation batch and RNA sequencing (RNA-seq) quality metrics (Methods). In total, we identified 943 differentially expressed genes at 24 h, 1,520 differentially expressed genes at 48 h and no differentially expressed genes after 72 h of reoxygenation (Fig. 1f; false discovery rate (FDR) ≤ 0.05 , fold change ≥ 1.5 ; hCS from three hiPS cell lines in two differentiation experiments; Supplementary Table 3). Among the differentially expressed genes were transcripts associated with a hypoxic response, such as *PLOD2* ($P = 0.006$), *PFKP* ($P = 0.008$),

PDK1 ($P = 0.0005$) and *IGFBP2* ($P = 0.0002$) (Fig. 1f), which we validated by quantitative PCR (qPCR) (Extended Data Fig. 2b and Supplementary Table 4). Interestingly, we also observed several genes associated with dorsal forebrain progenitors, such as *EOMES* (also known as *TBR2*) ($P = 0.006$) and *EMX1* ($P = 0.02$), as well as the cell cycle-related genes *ASPM* ($P = 0.002$) and *CENPF* ($P < 0.0001$) (Fig. 1f and Extended Data Fig. 2c). To gain insights into potential cell-type-specific changes following exposure to low oxygen, we assessed whether the combined set of differentially expressed genes was enriched for genes identified as being specifically expressed in laser-microdissected regions of the developing human cortex¹⁶. Overlap of the hypoxia-induced differentially expressed in hCS (1,754 unique genes) and subregions of the human cerebral cortex at PCW 21 revealed twofold enrichment for transcripts specifically expressed in the subventricular zone (SVZ) ($P < 10^{-7}$; Fig. 1g), a proliferative region bordering the ventricular epithelium that has undergone significant expansion in primates⁶ and where proliferation and neurogenesis continue until later stages of gestation^{12–14}.

On the basis of this observation, we next assessed whether exposure of hCS to low oxygen is associated with changes in the cortical

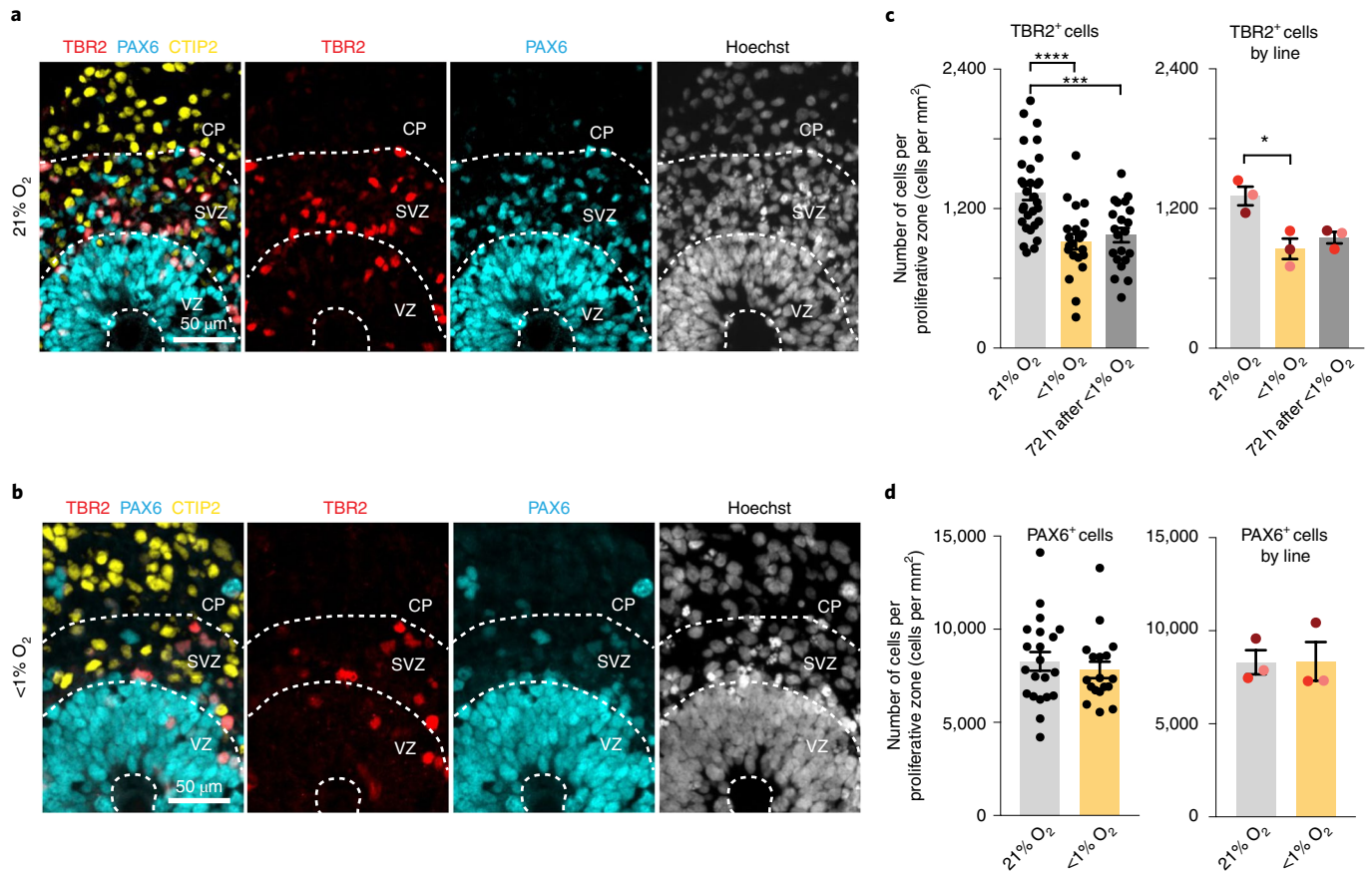


Fig. 2 | Proportion of TBR2⁺ cells in hCS exposed to low oxygen. **a, b**, Representative images of proliferative areas in hCS maintained in 21% O₂ (**a**) or exposed to <1% O₂ for 48 h (**b**). The VZ-, SVZ- and cortical plate-like areas are delineated by the patterns of expression of PAX6, TBR2 and CTIP2, and the density and orientation of nuclei (labeled with Hoechst). **c**, Quantification of the density of TBR2⁺ cells in hCS after 48 h of exposure to <1% O₂ and after 72 h of reoxygenation versus unexposed hCS (21% O₂). Data are shown as averages across individual hCS proliferative zones from three hiPS cell lines per condition (left, $n = 30$ areas for 21% O₂, $n = 21$ areas for <1% O₂, $n = 21$ areas for reoxygenation; one-way analysis of variance (ANOVA), $F_{2,69} = 13.64$, $P < 0.0001$; Dunnett's multiple-comparison test versus 21% O₂, **** $P < 0.0001$ for <1% O₂, *** $P = 0.0003$ for 72 h after <1% O₂), or as averages across different hiPS cell lines (right, $n = 3$ hiPS cell lines; one-way ANOVA, $F_{2,4} = 8.38$, $P = 0.03$; Dunnett's multiple-comparison test versus 21% O₂, * $P = 0.03$ for <1% O₂, $P = 0.06$ for 72 h after <1% O₂; each line is shown in a different color). **d**, Quantification of the density of PAX6⁺ cells in hCS after 48 h exposure to <1% O₂. Data are shown as averages across individual hCS proliferative zones from three hiPS cell lines per condition (left, $n = 21$ areas for 21% O₂ versus $n = 18$ areas for <1% O₂; two-tailed Mann-Whitney U test, $P = 0.44$) or as averages across different hiPS cell lines (right, $n = 3$ hiPS cell lines; Wilcoxon test, $P > 0.99$ for all comparisons; each line is shown in a different color). Data are the mean \pm s.e.m., and individual values are indicated by dots.

progenitors present in the SVZ, such as intermediate progenitors that are characterized by expression of the key transcription factor TBR2. At this *in vitro* stage, hCS display an internal cytoarchitecture consisting of PAX6⁺ radial glial cells organized in ventricular-like zones (VZ) around a lumen⁹ (Fig. 2a,b). These regions are surrounded by an intermediate region rich in TBR2⁺ cells resembling the SVZ, which is in turn surrounded by a cortical plate region containing mostly deep-layer neurons expressing the marker CTIP2 (also known as BLC11B). We used immunocytochemistry in hCS cryosections for PAX6, TBR2 and CTIP2 to delineate the proliferative VZ-like and SVZ-like regions from the cortical plate-like domain, as previously described in a cortical organoid system¹⁷. We quantified data from hCS derived from three hiPS cell lines in independent differentiations and observed that the density of TBR2⁺ cells per proliferative region was reduced by approximately 35% in hCS exposed for 48 h to <1% O₂ (left, $P < 0.0001$; right, $P = 0.03$), and this trend persisted at 72 h after reoxygenation (left, $P = 0.0003$; right, $P = 0.06$) (Fig. 2c). By contrast, the density of PAX6⁺ cells in the same delineated regions was not affected after 48 h of exposure to low oxygen (left, $P = 0.44$; right, $P > 0.99$; Fig. 2d), and the overall density of cells labeled with the nuclear dye Hoechst was unchanged

(left, $P = 0.09$; right, $P = 0.50$; Extended Data Fig. 3a). This reduction in TBR2⁺ cells, but not in PAX6⁺ cells, was also observed when we counted the raw, total number of TBR2⁺ (left, $P < 0.0001$; right, $P = 0.03$) or PAX6⁺ (left, $P = 0.44$; right, $P = 0.25$) cells out of all Hoechst-labeled nuclei in multiple whole cryosections of hCS (Extended Data Fig. 3b,c). Moreover, the affected population of TBR2⁺ cells was not the population of SVZ progenitors coexpressing SOX2 as investigated before in a mouse model¹⁸ (left, $P = 0.82$; right, $P = 0.06$; Extended Data Fig. 3d).

To gain insights into this potential cell-type-specific vulnerability of cortical progenitors following exposure to low oxygen, we turned back to the hypoxia-induced transcriptional changes in hCS. It has previously been demonstrated that the transcriptome has a reproducible coexpression structure that provides a framework for understanding disease biology^{19,20}. Therefore, we applied weighted gene coexpression network analysis (WGCNA)²¹ to identify modules of genes that changed with similar patterns following exposure to low oxygen in hCS (Fig. 3a). WGCNA identified nine gene coexpression modules correlated with low-oxygen exposure (FDR ≤ 0.05). These are referred to by color label identifiers; each represents a cluster of genes with a common expression pattern

across samples (Extended Data Fig. 4a,b). Blue and turquoise were the most strongly associated modules (Fig. 3b and Extended Data Fig. 4a,b). The blue module is enriched for genes associated with the hypoxic response pathway and genes regulated by HIF-1 α (Extended Data Fig. 4c; FDR \leq 0.0001). By contrast, the turquoise module was enriched for genes associated with the UPR, such as *PERK* ($P=0.03$), *ATF3* ($P=0.03$) and *XBPIs* ($P=0.04$). Analysis by qPCR confirmed these changes (Extended Data Fig. 4d and Supplementary Table 4).

The UPR pathway is a protective cellular response induced during periods of cellular stress that aims to restore protein homeostasis²². In certain cancer cells, hypoxia can activate components of the UPR pathway²³. Interestingly, previous work has linked the UPR to the generation of Tbr2⁺ intermediate progenitors in rodents²⁴. To verify whether the transcriptional changes in the UPR pathway are relevant to the TBR2-related phenotype after exposure to low oxygen, we exposed hCS to a potent small molecule called integrated stress response inhibitor (ISRIB), which reverses with high specificity the effects of eukaryotic initiation factor 2 α phosphorylation and restores protein translation while maintaining some of the protective effects of the integrated cellular response and the UPR^{25–27}. We observed that adding 10 nM ISRIB during the 48 h of exposure of hCS to <1% O₂ restored the density of TBR2⁺ cells (left, $P=0.30$; right, $P=0.45$ for <1% O₂ with ISRIB versus 21% O₂; Fig. 3c). Moreover, while the UPR-pathway-related transcription factor ATF4 was coexpressed by a larger proportion of TBR2⁺ cells in hCS exposed to low oxygen for 48 h versus hCS maintained at 21% O₂, this effect was restored with 10 nM ISRIB (left and right, $P>0.99$) and was partially restored 72 h after reoxygenation (left, $P=0.001$;

right, $P=0.51$) (Fig. 3d,e). At the same time, radial glia expressing PAX6 did not show an increase in ATF4 coexpression (left, $P=0.70$; right, $P=0.48$), and this remained unchanged by exposure to ISRIB (left, $P=0.54$; right, $P=0.21$) (Extended Data Fig. 5a). To further investigate the role of UPR, we exposed hCS for 48 h to 1.2 μ M tunicamycin, which has been shown to induce the UPR in the developing brain²⁸. Similarly to exposure to low oxygen, tunicamycin reduced the proportion of TBR2⁺ cells (left, $P<0.0001$; right, $P=0.01$; Fig. 3f). Moreover, the proportion of PAX6⁺ cells was not affected by exposure to tunicamycin (left, $P=0.37$; right, $P=0.20$; Extended Data Fig. 5b). Together, these experiments indicate that a 48 h exposure to low oxygen leads to a reduction in TBR2⁺ intermediate progenitors but not in PAX6⁺ radial glia, and that this phenotype can be prevented by simultaneous exposure to a nanomolar concentration of a UPR-pathway modulator.

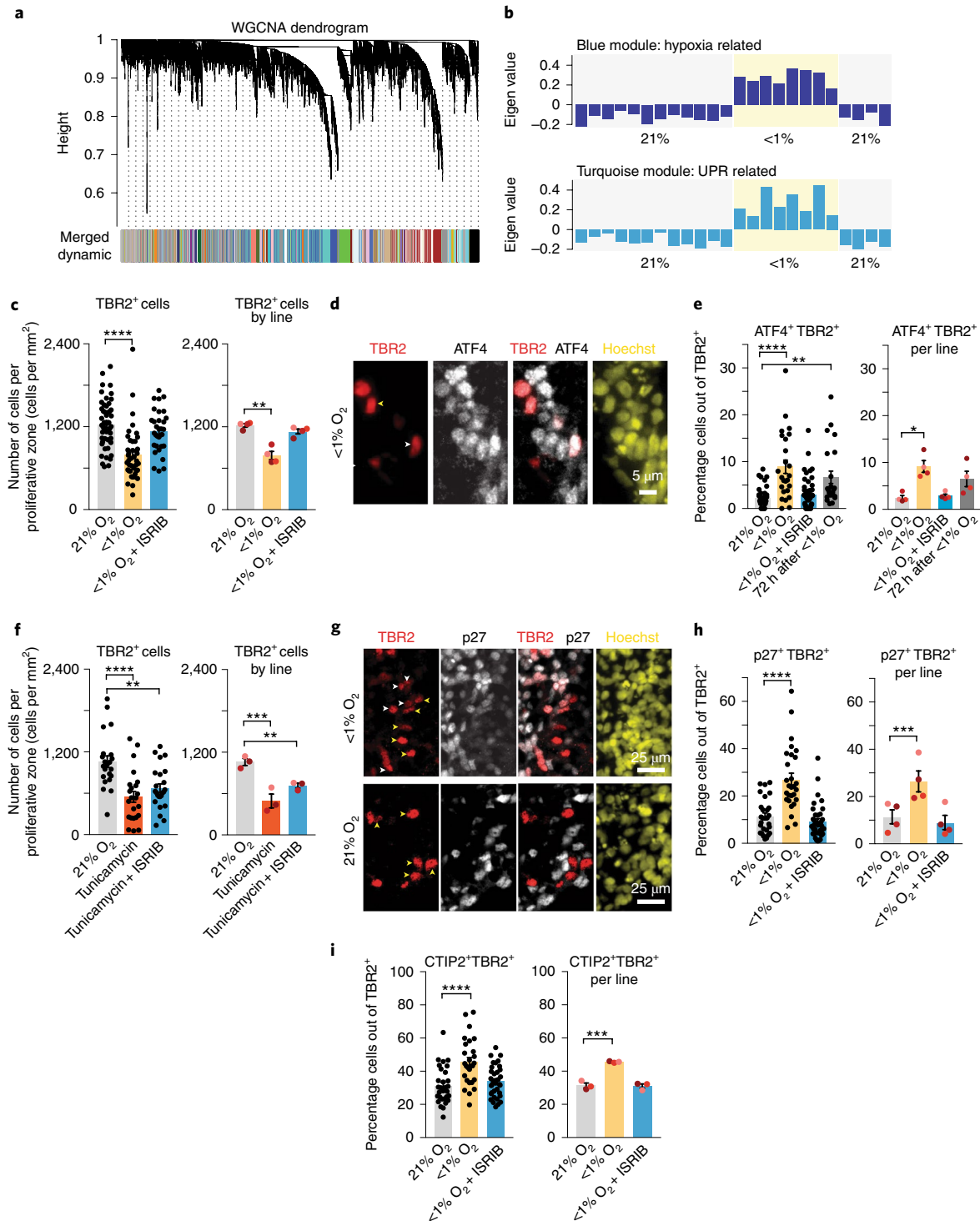
We did not observe significant cell death in hCS after 48 h of hypoxia (Extended Data Fig. 1b,c, Supplementary Table 2) and only approximately 0.1% of TBR2⁺ cells were c-CAS3⁺ in hCS cryosections ($P>0.99$; Extended Data Fig. 5c). Moreover, the unique set of 815 differentially expressed genes downregulated across 24 and 48 h are enriched for genes involved in the cell cycle (143 total genes, fold enrichment 2.47, Bonferroni FDR = 6.5×10^{-21}) (Fig. 1f). Therefore, we explored whether this reduction is related to changes in the cell cycle. Co-staining with p27, a protein that regulates G1 and helps cells withdraw from the cell cycle when they terminally differentiate, showed a 2.4-fold increase in the overlap with TBR2⁺ cells following exposure to low oxygen (left, $P<0.0001$; right, $P=0.0006$), and this effect was prevented by simultaneous exposure to ISRIB (left, $P=0.54$; right, $P=0.43$) (Fig. 3g,h). At the same time,

Fig. 3 | Unfolded protein response pathway in hCS exposed to low oxygen. **a**, Dendrogram for the WGCNA, which identified genes with similar expression profiles and grouped them into modules (represented by colors). **b**, Eigengene expression profiles ('average' expression profile of all module genes) for the top WGCNA modules associated with exposure of hCS to low oxygen for 48 h. The blue module (top) contains genes strongly enriched for annotation in biological pathways related to the hypoxia response (HIF-1 α transcription-factor network), while the turquoise module (bottom) is enriched for genes involved in the UPR pathway. **c**, Quantification of the density of TBR2⁺ cells in hCS after 48 h exposure to <1% O₂ in the presence or absence of 10 nM ISRIB. Data are shown as averages across individual hCS proliferative zones from four hiPS cell lines per condition (left, $n=50$ areas for 21% O₂ versus $n=42$ areas for <1% O₂ versus $n=32$ areas for <1% O₂ with ISRIB; one-way ANOVA test, $F_{2,21}=15.85$, $P<0.0001$; Dunnett's multiple-comparison test versus 21% O₂, **** $P<0.0001$ for <1% O₂, $P=0.30$ for <1% O₂ + ISRIB) or as averages across different hiPS cell lines (right, $n=4$ hiPS cell lines; one-way ANOVA test, $F_{2,6}=13.43$, $P=0.006$; Dunnett's multiple-comparison test versus 21% O₂, ** $P=0.004$ for <1% O₂, $P=0.45$ for <1% O₂ + ISRIB; each line is shown in a different color). **d**, Representative images of cells coexpressing ATF4 and TBR2 in hCS exposed to <1% O₂ for 48 h. The yellow arrow shows an example of TBR2⁺ATF4⁺; the white arrow shows an example of cells that are TBR2⁺ATF4⁻. **e**, Quantification of the percentage of cells coexpressing ATF4 and TBR2 in cryosections of hCS after 48 h exposure to <1% O₂ in the presence or absence of 10 nM ISRIB and after 72 h of reoxygenation. Data are shown as averages across individual hCS cryosections from four hiPS cell lines per condition ($n=36$ sections for 21% O₂, $n=25$ sections for <1% O₂, $n=48$ sections for <1% O₂ + ISRIB, $n=23$ sections for reoxygenation; Kruskal-Wallis test, $P<0.0001$; Dunn's multiple-comparison test versus 21% O₂, **** $P<0.0001$ for <1% O₂, $P>0.99$ for <1% O₂ + ISRIB, ** $P=0.001$ for 72 h after <1% O₂) or as averages across different hiPS cell lines (right, $n=4$ hiPS cell lines; Friedman's test, $P=0.01$; Dunnett's multiple-comparison test versus 21% O₂, * $P=0.01$ for <1% O₂, $P>0.99$ for <1% O₂ + ISRIB, $P=0.51$ for 72 h after <1% O₂; each line is shown in a different color). **f**, Quantification of the density of TBR2⁺ cells in hCS after exposure for 48 h to 1.2 μ M tunicamycin in the presence or absence of 10 nM ISRIB. Data are shown as averages across individual hCS proliferative zones from three hiPS cell lines per condition (left, $n=22$ areas for 21% O₂, $n=23$ areas for tunicamycin, $n=24$ areas for tunicamycin + ISRIB; one-way ANOVA, $F_{2,66}=12.69$, $P<0.0001$; Dunnett's multiple-comparison test versus 21% O₂, **** $P<0.0001$ for Tunicamycin; *** $P=0.003$ for Tunicamycin + ISRIB), or as averages across different hiPS cell lines (right, $n=3$ hiPS cell lines; one-way ANOVA $F_{2,4}=11.85$, $P=0.02$; with Dunnett's multiple-comparison test versus 21% O₂, * $P=0.01$ for Tunicamycin; * $P=0.03$ for Tunicamycin + ISRIB; each line is shown in a different color). **g**, Representative images of cells coexpressing p27 and TBR2 in cryosections of hCS after exposure to 48 h of <1% O₂ in the presence or absence of 10 nM ISRIB. Yellow arrows show examples of TBR2⁺p27⁻ cells; white arrows show examples of cells that are TBR2⁺p27⁺. **h**, Quantification of the percentage of cells coexpressing p27 and TBR2 in cryosections of hCS after 48 h of exposure to <1% O₂ in the presence or absence of 10 nM ISRIB. Data are shown as averages across individual hCS cryosections from four hiPS cell lines per condition ($n=27$ sections for 21% O₂ and $n=28$ sections for <1% O₂ versus $n=36$ sections for <1% O₂ + ISRIB; Kruskal-Wallis test, $P<0.0001$; Dunn's multiple-comparison test versus 21% O₂, **** $P<0.0001$ for <1% O₂, $P=0.54$ for <1% O₂ + ISRIB), or as averages across different hiPS cell lines (right, $n=4$ hiPS cell lines; one-way ANOVA $F_{2,6}=43.78$, $P=0.0003$; Dunnett's multiple-comparison test versus 21% O₂, *** $P=0.0006$ for <1% O₂, $P=0.43$ for <1% O₂ + ISRIB; each line is shown in a different color). **i**, Quantification of the percentage of cells coexpressing CTIP2 (also known as BCL11B) and TBR2 in cryosections of hCS after 48 h of exposure to <1% O₂ in the presence or absence of 10 nM ISRIB. Data are shown as averages across individual hCS cryosections from three hiPS cell lines per condition ($n=30$ sections for 21% O₂, $n=27$ sections for <1% O₂, $n=34$ sections for <1% O₂ + ISRIB; one-way ANOVA, $F_{2,88}=12.31$, $P<0.0001$; Dunnett's multiple-comparison test versus 21% O₂, **** $P<0.0001$ for <1% O₂, $P=0.58$ for <1% O₂ + ISRIB), or as averages across different hiPS cell lines (right, $n=3$ hiPS cell lines; one-way ANOVA $F_{2,6}=53.67$; $P=0.0001$, Dunnett's multiple-comparison test versus 21% O₂, *** $P=0.0002$ for <1% O₂, $P=0.96$ for <1% O₂ + ISRIB; each line is shown in a different color). Data are the mean \pm s.e.m.; individual values are indicated by dots.

few PAX6⁺ radial glia in hCS coexpressed p27, and this proportion did not change after oxygen deprivation (left, $P=0.88$; right, $P=0.67$) or ISRIB exposure (left, $P=0.90$; right, $P=0.94$) (Extended Data Fig. 5d). To explore whether this increase in p27 expression was associated with changes in proliferation, we costained TBR2⁺ cells with the cell cycle marker Ki67 (left, $P=0.91$; right, $P=0.91$) and the mitotic marker PH3 (left, $P=0.55$; right, $P=0.56$) but did not find differences after exposure to low oxygen (Extended Data Fig. 5e–g). Alternatively, these changes in p27 may be associated with cell cycle exit and early neural differentiation. Therefore, we quantified the percentage of TBR2⁺ cells that coexpressed the

cortical marker CTIP2 and found an increase by approximately 50% in double-positive cells (left, $P<0.0001$; right, $P=0.0002$), which was prevented by exposure to 10 nM ISRIB (left, $P=0.58$; right, $P=0.96$) (Fig. 3i). This suggests that TBR2⁺ cells may be particularly susceptible to premature differentiation after exposure to low oxygen levels and that modulators of the UPR pathways could be used to restore hypoxia-related defects in cortical progenitor subtypes.

Finally, to validate these findings in a more physiological system, we used primary human cortical tissue at PCW 20, which we sectioned and then exposed to either <1% O₂ or 21% O₂ for 48 h in



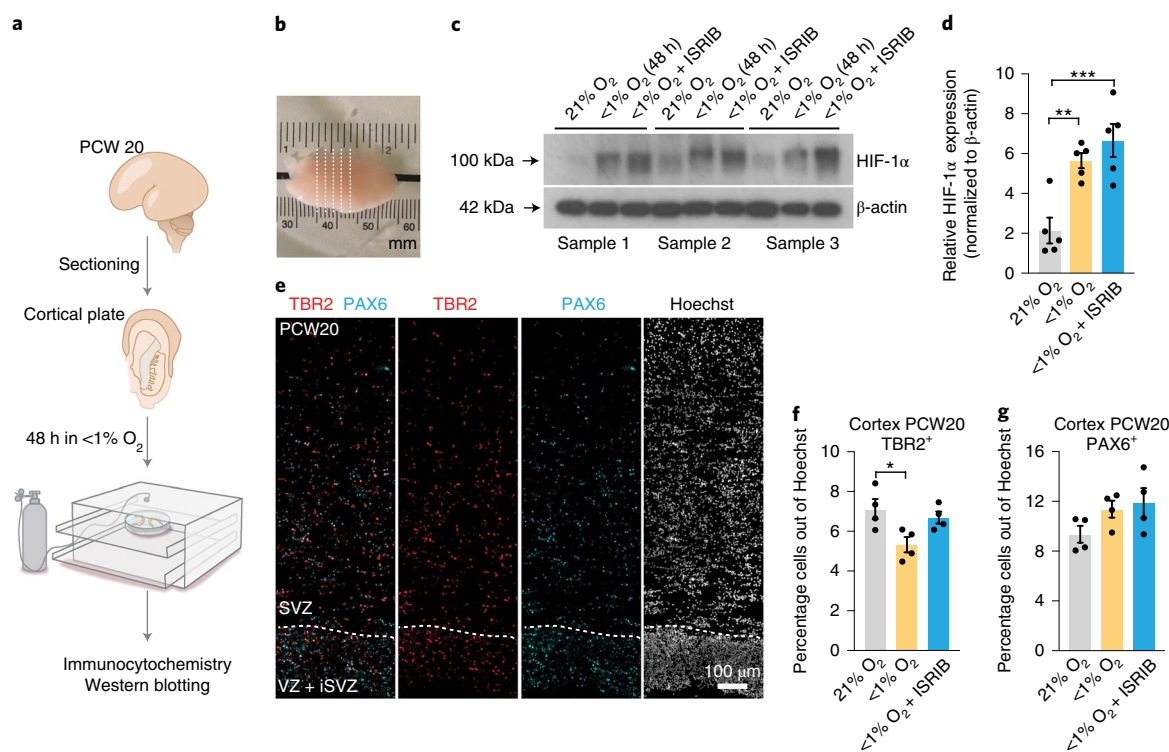


Fig. 4 | Validation in primary human cortical tissue in vitro. **a**, Scheme showing sectioning and gas chamber exposure to low oxygen of human cortical tissue (approximately PCW 20). **b**, Macroscopic image of cortical tissue and sectioning. Dashed lines indicate approximate regions of sectioning for slice culture. **c,d**, Representative western blots and quantification of HIF-1 α protein expression in human cortical sections (PCW 20) after 48 h exposure to <1% O₂ with or without 10 nM ISRIB; normalized to β -actin ($n=5$ slices; one-way ANOVA $F_{2,8}=19.39$, $P=0.0009$; Dunnett's multiple-comparison test versus 21% O₂, ** $P=0.003$ for <1% O₂, *** $P=0.0007$ for <1% O₂ + ISRIB). Western blots were cropped to show the relevant bands; molecular weight markers are indicated on the left (in kDa). See Supplementary Table 2 for quantifications. Uncropped blots are available as source data. **e**, Image of proliferative zones (VZ and SVZ) in cortical primary tissue delineated by expression of PAX6, TBR2 and Hoechst. **f**, Quantification of the density of TBR2⁺ cells in cryosections of primary human fetal tissue after 48 h exposure to <1% O₂ in the presence or absence of 10 nM ISRIB ($n=4$ sections; one-way ANOVA, $F_{2,9}=5.32$, $P=0.02$; Dunnett's multiple-comparison test versus 21% O₂, * $P=0.02$ for <1% O₂, $P=0.69$ for <1% O₂ + ISRIB). **g**, Quantification of density of the PAX6⁺ cells in cryosections of primary human fetal tissue after 48 h exposure to <1% O₂ in the presence or absence of 10 nM ISRIB ($n=4$ sections; one-way ANOVA, $F_{2,9}=2.29$, $P=0.15$; Dunnett's multiple-comparison test versus 21% O₂, $P=0.23$ for <1% O₂, $P=0.12$ for <1% O₂ + ISRIB). Data are the mean \pm s.e.m. Individual values are indicated by dots.

a gas-controlled environmental chamber (Fig. 4a,b). Western blot analysis showed that HIF-1 α protein stabilized at 48 h in low oxygen ($P=0.003$) and this effect was present even after simultaneous exposure to 10 nM ISRIB ($P=0.0007$) (Fig. 4c,d and Supplementary Table 2). We next performed immunostaining for PAX6 and TBR2 in cortical slices to delineate the proliferative VZ-like and SVZ-like + outer SVZ-like areas (Fig. 4e). We found a decrease in the proportion of TBR2⁺ cells following exposure to low oxygen ($P=0.02$) and this was prevented by simultaneous exposure to 10 nM ISRIB ($P=0.69$) (Fig. 4f). At the same time, the proportion of PAX6⁺ cells was unchanged in the absence ($P=0.23$) or presence ($P=0.12$) of ISRIB (Fig. 4g).

In this study, we show how hiPS cell-derived 3D brain cultures can be used to model injury in the developing brain. There are several new aspects to this work. First, we used a reproducible brain-region-specific organoid model that recapitulates key features of the mid-gestation human cortex^{8–10}, and we validate our findings in slices of human cortex. This platform could serve both as a model of hypoxic encephalopathy of prematurity and as a model of second-trimester placental insufficiency. Recent data in human brain tissue have demonstrated continued neurogenesis into the third trimester of pregnancy^{12–14}. In fact, the risk for encephalopathy of prematurity is highest in extremely preterm infants and the neurodevelopmental consequences are most severe for this patient population⁴.

Second, we find that TBR2⁺ progenitors, a population of amplifying cells that reside in the SVZ and that are thought to contribute to expansion of the neocortex by increasing neuron number, are particularly affected by oxygen deprivation. In fact, TBR2⁺ progenitors are positioned close to blood vessels²⁹, and increased oxygen tension in the rodent cortex results in expansion of the SVZ¹⁸. While other studies have investigated the role of oxygen on dissociated human radial glia³⁰, the effect of hypoxia on human TBR2⁺ progenitors has not been explored. Future studies using this system should investigate the susceptibility of outer radial glia, which are more transcriptionally similar to radial glia but reside in the expanded outer SVZ in humans³¹. Moreover, it remains to be established how changes in specific progenitors affect brain development, as previous studies in premature brains have indicated an impact on glutamatergic neurogenesis and gray matter¹⁴. Third, we find that these cell-type-specific defects are related to the UPR, and in particular to the PERK-eIF2 α -ATF4 pathway. This endoplasmic reticulum stress-response pathway controls protein homeostasis and has been associated with hypoxia in cancer²³ and more recently with cortical development³². Components of the UPR pathway correlate with milestones in corticogenesis, and changes in the UPR in rodents affect Tbr2⁺ cells²⁴. More specifically, loss of a component of the elongator complex leads to impaired translation speed, triggers the UPR and reduces the number of Tbr2⁺ cells²⁴. Therefore, hypoxia-related UPR changes in intermediate progenitors could result in

cell-cycle changes and premature neural differentiation. Fourth, we show that the UPR modulator ISRIB—a small molecule with good pharmacokinetic properties that permeates the blood–brain barrier²⁵—prevents the oxygen-related TBR2 defects in hCS and in human tissue. Future studies should validate this effect in other models to evaluate translational potential and investigate the effect of genotype on hypoxia susceptibility and recovery.

There are several limitations to our study. Our hCS system does not include immune cells and is not vascularized, and therefore the inflammation component of encephalopathy of prematurity is not captured here³³. Future assembloid models could incorporate microglia and other cells³⁴ to study their contributions to encephalopathy of prematurity. Although oxygen concentration in the cerebral circulation increases following premature birth³⁵ and our goal was to model postnatal hypoxia in the premature brain, hCS derivation and maintenance are pursued at atmospheric oxygen levels. We have shown that hCS can be maintained in vitro for hundreds of days to model late stages of development to include astrocytes that resemble primary postnatal astrocytes¹¹. Therefore, future studies could use this system to model brain injury at later in utero stages. Postmortem studies have indicated a significant loss of GABAergic interneurons in premature infants^{36,37}. Our current model does not include interneurons, which are born in the ventral forebrain and have to migrate dorsally to integrate into cortical circuits³⁸. Therefore, future studies could use forebrain assembloids that combine dorsal and ventral forebrain organoids to model migration³⁹. Similarly, organoid models that include oligodendrocytes together with astrocytes and neurons could be combined with the hypoxia platform we are describing to model myelination defects⁴⁰.

The use of 3D brain organoids or assembloids holds great promise for the study of the interaction of environmental factors impacting brain development. Moreover, this personalized, scalable human system could dissect individual susceptibility and protective factors and therefore may ultimately identify therapeutics strategies to bridge the disconnect between medical advances and neurodevelopmental outcomes in neonatology.

Online content

Any methods, additional references, Nature Research reporting summaries, source data, statements of code and data availability and associated accession codes are available at <https://doi.org/10.1038/s41591-019-0436-0>.

Received: 22 March 2018; Accepted: 25 March 2019;
Published online: 6 May 2019

References

- Penn, A. A., Gressens, P., Fleiss, B., Back, S. A. & Gallo, V. Controversies in preterm brain injury. *Neurobiol. Dis.* **92**, 90–101 (2016).
- Volpe, J. J. Brain injury in premature infants: a complex amalgam of destructive and developmental disturbances. *Lancet Neurol.* **8**, 110–124 (2009).
- Volpe, J. J. The encephalopathy of prematurity—brain injury and impaired brain development inextricably intertwined. *Semin. Pediatr. Neurol.* **16**, 167–178 (2009).
- Jarjour, I. T. Neurodevelopmental outcome after extreme prematurity: a review of the literature. *Pediatr. Neurol.* **52**, 143–152 (2015).
- Salmaso, N., Jablonska, B., Scaffidi, J., Vaccarino, F. M. & Gallo, V. Neurobiology of premature brain injury. *Nat. Neurosci.* **17**, 341–346 (2014).
- Sousa, A. M. M., Meyer, K. A., Santpere, G., Gulden, F. O. & Sestan, N. Evolution of the human nervous system function, structure, and development. *Cell* **170**, 226–247 (2017).
- Pasca, S. P. The rise of three-dimensional human brain cultures. *Nature* **553**, 437–445 (2018).
- Sloan, S. A., Andersen, J., Pasca, A. M., Birey, F. & Pasca, S. P. Generation and assembly of human brain region-specific three-dimensional cultures. *Nat. Protoc.* **13**, 2062–2085 (2018).
- Pasca, A. M. et al. Functional cortical neurons and astrocytes from human pluripotent stem cells in 3D culture. *Nat. Methods* **12**, 671–678 (2015).
- Yoon, S. J. et al. Reliability of human cortical organoid generation. *Nat. Methods* **16**, 75–78 (2019).
- Sloan, S. A. et al. Human astrocyte maturation captured in 3D cerebral cortical spheroids derived from pluripotent stem cells. *Neuron* **95**, 779–790 (2017).
- Arshad, A. et al. Extended production of cortical interneurons into the third trimester of human gestation. *Cereb. Cortex* **26**, 2242–2256 (2016).
- Zecevic, N., Chen, Y. & Filipovic, R. Contributions of cortical subventricular zone to the development of the human cerebral cortex. *J. Comp. Neurol.* **491**, 109–122 (2005).
- Malik, S. et al. Neurogenesis continues in the third trimester of pregnancy and is suppressed by premature birth. *J. Neurosci.* **33**, 411–423 (2013).
- Carreau, A., El Hafny-Rahbi, B., Matejuk, A., Grillon, C. & Kieda, C. Why is the partial oxygen pressure of human tissues a crucial parameter? Small molecules and hypoxia. *J. Cell. Mol. Med.* **15**, 1239–1253 (2011).
- Miller, J. A. et al. Transcriptional landscape of the prenatal human brain. *Nature* **508**, 199–206 (2014).
- Bershteyn, M. et al. Human iPSC-derived cerebral organoids model cellular features of lissencephaly and reveal prolonged mitosis of outer radial glia. *Cell Stem Cell* **20**, 435–449 (2017).
- Wagenfuhr, L., Meyer, A. K., Braunschweig, L., Marrone, L. & Storch, A. Brain oxygen tension controls the expansion of outer subventricular zone-like basal progenitors in the developing mouse brain. *Development* **142**, 2904–2915 (2015).
- Stuart, J. M., Segal, E., Koller, D. & Kim, S. K. A gene-coexpression network for global discovery of conserved genetic modules. *Science* **302**, 249–255 (2003).
- Voineagu, I. et al. Transcriptomic analysis of autistic brain reveals convergent molecular pathology. *Nature* **474**, 380–384 (2011).
- Zhang, B. & Horvath, S. A general framework for weighted gene co-expression network analysis. *Stat. Appl. Genet. Mol. Biol.* **4**, Article17 (2005).
- Wang, M. & Kaufman, R. J. Protein misfolding in the endoplasmic reticulum as a conduit to human disease. *Nature* **529**, 326–335 (2016).
- Fels, D. R. & Koumenis, C. The PERK/eIF2 α /ATF4 module of the UPR in hypoxia resistance and tumor growth. *Cancer Biol. Ther.* **5**, 723–728 (2006).
- Laguesse, S. et al. A dynamic unfolded protein response contributes to the control of cortical neurogenesis. *Dev. Cell* **35**, 553–567 (2015).
- Sidrauski, C. et al. Pharmacological brake-release of mRNA translation enhances cognitive memory. *eLife* **2**, e00498 (2013).
- Sidrauski, C. et al. Pharmacological dimerization and activation of the exchange factor eIF2B antagonizes the integrated stress response. *eLife* **4**, e07314 (2015).
- Zyryanova, A. F. et al. Binding of ISRIB reveals a regulatory site in the nucleotide exchange factor eIF2B. *Science* **359**, 1533–1536 (2018).
- Wang, H. et al. Tunicamycin-induced unfolded protein response in the developing mouse brain. *Toxicol. Appl. Pharmacol.* **283**, 157–167 (2015).
- Javaherian, A. & Kriegstein, A. A stem cell niche for intermediate progenitor cells of the embryonic cortex. *Cereb. Cortex* **19** (Suppl 1), i70–i77 (2009).
- Ortega, J. A., Sirois, C. L., Memi, F., Glidden, N. & Zecevic, N. Oxygen levels regulate the development of human cortical radial glia cells. *Cereb. Cortex* **27**, 3736–3751 (2017).
- Pollen, A. A. et al. Molecular identity of human outer radial glia during cortical development. *Cell* **163**, 55–67 (2015).
- Godin, J. D., Creppe, C., Laguesse, S. & Nguyen, L. Emerging roles for the unfolded protein response in the developing nervous system. *Trends Neurosci.* **39**, 394–404 (2016).
- Jantzie, L. L. & Robinson, S. Preclinical models of encephalopathy of prematurity. *Dev. Neurosci.* **37**, 277–288 (2015).
- Amin, N. D. & Pasca, S. P. Building models of brain disorders with three-dimensional organoids. *Neuron* **100**, 389–405 (2018).
- Soothill, P. W., Nicolaides, K. H., Rodeck, C. H. & Gamsu, H. Blood gases and acid-base status of the human second-trimester fetus. *Obstet. Gynecol.* **68**, 173–176 (1986).
- Lacaille, H. et al. Impaired interneuron development in a novel model of neonatal brain injury. *eNeuro* **6**, 0300–0318 (2019).
- Robinson, S., Li, Q., Dechant, A. & Cohen, M. L. Neonatal loss of γ -aminobutyric acid pathway expression after human perinatal brain injury. *J. Neurosurg.* **104**, 396–408 (2006).
- Paredes, M. F. et al. Extensive migration of young neurons into the infant human frontal lobe. *Science* **354**, aaf7073 (2016).
- Birey, F. et al. Assembly of functionally integrated human forebrain spheroids. *Nature* **545**, 54–59 (2017).
- Marton, R. M. et al. Differentiation and maturation of oligodendrocytes in human three-dimensional neural cultures. *Nat. Neurosci.* **22**, 484–491 (2019).

Acknowledgements

We thank W.E. Benitz, D.K. Stevenson, V. K. Bhutani and U. Francke for valuable scientific advice and discussions. This work was supported by the US National Institute

of Health (NIH) BRAINS Award (MH107800), the MQ Fellow Award, the NYSCF Robertson Stem Cell Investigator Award, the Stanford Neurosciences Institute's Human Brain Organogenesis Program and the Brain Rejuvenation Project, Stanford Bio-X, the Kwan Research Fund and the California Institute of Regenerative Medicine (CIRM) (to S.P.P.); the UCSF Weill Institute for Neurosciences (startup funds to A.J.W.); NIH R01MH108659 and R01MH108659 (to T.D.P.); and the NIH K12-HD000850 (Pediatric Scientist Development Program), the Association of Medical School Pediatric Department Chairs (AMSPDC) and Stanford Maternal and Child Health Research Institute Fellowship (to A.M.P.).

Author contributions

A.M.P. and J.-Y. P. performed the neural differentiation and hypoxia experiments. A.M.P., J.-Y.P., H.-W.S., O.R., Q.Q., R.K., A.J.W., R.O. and T.D.P. carried out experiments, analyzed data or contributed critical reagents. A.M.P. and S.P.P. wrote the manuscript with input from all authors. S.P.P. supervised the work.

Competing interests

Stanford University has filed a provisional patent application that covers the generation of region-specific brain organoids from pluripotent stem cells (US Application Serial No. 15/158,408) (A.M.P. and S.P.P.).

Additional information

Extended data is available for this paper at <https://doi.org/10.1038/s41591-019-0436-0>.

Supplementary information is available for this paper at <https://doi.org/10.1038/s41591-019-0436-0>.

Reprints and permissions information is available at www.nature.com/reprints.

Correspondence and requests for materials should be addressed to S.P.P.

Publisher's note: Springer Nature remains neutral with regard to jurisdictional claims in published maps and institutional affiliations.

© The Author(s), under exclusive licence to Springer Nature America, Inc. 2019

Methods

Culture of hiPS cells. The hiPS cell lines used in this study were validated using standardized methods as previously described^{39,41}. Cultures were tested for mycoplasma and maintained mycoplasma free. A total of five control hiPS cell lines were derived from fibroblasts collected from four subjects (three males and one female). Approval for this study was obtained from the Stanford IRB panel and informed consent was obtained from all subjects.

Generation of hCS from hiPS cells. hiPS cells were cultured on inactivated mouse embryonic fibroblast feeders (EmbryoMax PMEF; Millipore) in hiPS cell medium containing DMEM/F12 (1:1, Life Technologies, 11330), knockout serum (20%, Life Technologies, 10828), non-essential amino acids (1 mM, Life Technologies, 11140), GlutaMax (1:200, Life Technologies, 35050), β -mercaptoethanol (0.1 mM, Sigma-Aldrich, M3148), penicillin and streptomycin (1:100, Life Technologies, 15070), and supplemented with fibroblast growth factor 2 (10 ng ml^{-1} diluted in 0.1% BSA; R&D Systems). The generation of hCS from hiPS cells was performed as previously described⁹. To initiate the generation of hCS, intact hiPS cell colonies were lifted from the plates using dispase (0.35 mg ml^{-1}) and transferred to ultralow-attachment plastic dishes (Corning) in hiPS cell medium supplemented with the two SMAD inhibitors dorsomorphin ($5 \mu\text{M}$, Sigma-Aldrich) and SB-431542 ($10 \mu\text{M}$, Tocris) and the ROCK inhibitor Y-27632 ($10 \mu\text{M}$, EMD Chemicals). For the first 5 d, the hiPS cell medium was changed every day and supplemented with dorsomorphin and SB-431542. On the sixth day in suspension, neural spheroids were transferred to neural medium containing neurobasal-A (Life Technologies, 10888), B-27 supplement without vitamin A (Life Technologies, 12587), GlutaMax (1:100, Life Technologies), penicillin and streptomycin (1:100, Life Technologies) and supplemented with the growth factors epidermal growth factor (20 ng ml^{-1} ; R&D Systems) and fibroblast growth factor 2 (20 ng ml^{-1} ; R&D Systems) until day 24. From day 25 to day 42, the neural medium was supplemented with the growth factors brain-derived neurotrophic factor (20 ng ml^{-1} , Peprotech) and neurotrophin 3 (20 ng ml^{-1} , Peprotech) with medium changes every other day. From day 43 onward, hCS were maintained in unsupplemented neural medium with medium changes every 4–6 d. A step-by-step protocol describing hCS generation can also be found in ref. ⁸.

Exposure of hCS to low oxygen. Human cortical spheroids derived from five hiPS cell lines (four individuals) were used for low-oxygen exposure in a total of nine independent experiments. At 74–78 d of in vitro differentiation, hCS maintained in 21% O_2 and 5% CO_2 were transferred to a C-chamber hypoxia sub-chamber (Biospherix) in neural medium (without growth factors) for 48 h. The medium was previously equilibrated for approximately 16 h at <1% O_2 , 5% CO_2 and 37°C. The level of oxygen was controlled using a Proox 110 Compact Oxygen Controller (Biospherix) and a mixed CO_2/N_2 compressed gas source. After 48 h, hCS were immediately collected for analyses or transferred to an incubator with 21% O_2 and 5% CO_2 for another 72 h (reoxygenation condition).

Exposure of hCS to tunicamycin. At 74–78 d of in vitro differentiation, hCS were exposed to $1.2 \mu\text{M}$ tunicamycin (Sigma, T7765) for 48 h at 21% O_2 and 5% CO_2 . After 48 h, hCS were collected for analyses as described for the hypoxia experiments.

Oxygen tension measurements. The oxygen optical microsensor OXB50 ($50 \mu\text{m}$, PyroScience) was used to measure oxygen tension in hCS. This sensor measures changes in oxygen tension by calculating the quenching of a probe (Red Flash Dye) situated at the tip of the sensor. The probe is excited with red light at a wavelength of 610–630 nm and shows an oxygen-dependent luminescence in the near-infrared spectrum (760–790 nm). A two-point calibration was performed before measurements. Pure nitrogen gas and ambient air were set as 0 and 100% air saturation. Optical signals were sampled and digitized by the compatible meter of the sensor (FireStingO2, PyroScience) and Oxygen Logger software (PyroScience). To determine the oxygen levels at various depths, we mounted the sensor on a micromanipulator with a high-precision slide ($<0.1 \mu\text{m}$ axial resolution) and applied 50- μm steps from the hCS surface toward the center.

Human tissue. Human tissue was obtained under a protocol approved by the Research Compliance Office at Stanford University. The tissue was immediately placed in RPMI medium and processed within 16 h of collection using a previously adapted protocol⁴². In brief, PCW 20 frontal brain tissue was embedded in 4% low-melting-point agarose in PBS and cut using a scalpel to obtain 2-mm-thick sections. The sections were then placed in tissue culture plates containing culture medium (66% BME, 25% Hanks, 5% FBS, 1% N-2, 1% penicillin, streptomycin and glutamine; all from Invitrogen) and 0.66% D-(+)-glucose (Sigma-Aldrich) and incubated in standard conditions (21% O_2 , 5% CO_2 , 37°C) for 24 h. Sections were subsequently exposed to <1% O_2 and 5% CO_2 in a chamber or maintained in 21% O_2 and 5% CO_2 for 48 h. Samples were then collected and processed for analyses.

Cryopreservation. Human cortical spheroids were fixed in 4% paraformaldehyde overnight. They were then washed in PBS and transferred to 30% sucrose for

48–72 h. Subsequently, they were transferred into embedding medium (Tissue-Tek OCT Compound 4583, Sakura Finetek), snap-frozen on dry ice and stored at -80°C . For immunohistochemistry, 10- μm -thick sections were cut using a cryostat (Leica).

Slices of primary cortical tissue (2 mm thick) were fixed in 4% paraformaldehyde for 48 h. They were then washed in PBS and transferred to 30% sucrose for 5 d. Subsequently, they were moved to embedding medium (1:1 mixture of 30% sucrose and Tissue-Tek OCT Compound 4583, Sakura Finetek), snap-frozen on dry ice and stored at -80°C . For immunohistochemistry, 40- μm -thick cryosections were cut using a Leica cryostat.

Immunocytochemistry. Cryosections of hCS were washed with PBS to remove excess OCT and blocked in 10% normal donkey serum (NDS), 0.3% Triton X-100 diluted in PBS for 1 h at room temperature. The sections were then incubated overnight at 4°C with primary antibodies diluted in PBS containing 2% NDS and 0.1% Triton X-100. PBS was used to wash off the primary antibodies and the cryosections were incubated with secondary antibodies in PBS with 2% NDS and 0.1% Triton X-100 for 1 h. After incubation with secondary antibodies, three washes of 15 min were performed in PBS. The following primary antibodies were used for immunohistochemistry: CTIP2 (rat, 1:300, Abcam, AB18465), p27 (rabbit, 1:100, Thermo Fisher Scientific, PA5-27188), ATF4 (rabbit, 1:50, Cell Signaling, D4B8, 11815), HIF-1 α (mouse, 1:50, Santa Cruz sc-53546), PAX6 (rabbit, 1:300, BioLegend, PRB-278P), SOX2 (rabbit, 1:200, Cell Signaling 3579 S), PH3 (rat, 1:500, Abcam AB10543), Ki67 (rabbit, 1:100, Novus Biological NB600-1252). For TBR2 staining (anti-TBR2, mouse, 1:100; R&D, MAB6166), antigen retrieval (using 10 mM sodium citrate and heating to 95°C) was performed for 20 min and sections were blocked in 0.1% Triton X-100, 10% serum and 0.2% gelatin for 1 h. The sections were incubated with primary antibodies in blocking buffer overnight at 4°C, then washed with PBS and incubated with secondary antibodies diluted in blocking buffer for 1 h at room temperature. After incubation with secondary antibodies, three washes of 15 min were performed in PBS.

Cryosections of primary cortical tissue were washed with PBS to remove excess OCT. Antigen retrieval (using 10 mM sodium citrate and heating to 95°C) was performed for 20 min. Cryosections were blocked in 0.1% Triton X-100, 10% NDS and 0.2% gelatin diluted in PBS for 4 h at room temperature. The sections were then incubated for 24 h at 4°C with primary antibodies diluted in blocking solution. Primary antibodies were washed off with 0.5% Triton X-100 diluted in PBS for 1 h and subsequently incubated with secondary antibodies in blocking solution for 2 h at room temperature. After incubation with secondary antibodies, three washes of 20 min were performed in PBS. The following primary antibodies were used for immunohistochemistry: PAX6 (rabbit, 1:300, Biolegend, PRB-278P), TBR2 (sheep, 1:100, Novus Biologicals, AF6166).

Secondary antibodies AlexaFluor 488, 568 and 647 (donkey anti-rabbit, anti-rat, anti-mouse or anti-sheep) were used at a 1:500 dilution. Nuclei were visualized with Hoechst 33258 (Life Technologies, 1:10,000). Cryosections were mounted for microscopy on glass coverslips, using Aquamount (Thermo Fisher Scientific) and imaged on a Zeiss M1 Axioscope (for hCS cryosections) or a Keyence BZ-X710 microscope (for primary cortical tissue cryosections).

Immunocytochemistry quantification. The density of TBR2⁺, PAX6⁺ and Hoechst⁺ cells was estimated in 10- μm -thick hCS cryosections. The number of cells was quantified in circular areas around proliferative zones. The boundary between proliferative zones (VZ and SVZ) and cortical plate was established on the basis of the expression, cell orientation and density of nuclei (Hoechst) and PAX6⁺ and CTIP2⁺ cells. Independently, the percentages of TBR2⁺ and PAX6⁺ cells were also quantified out of the total number of cells (Hoechst⁺) in whole 10- μm -thick cryosections of hCS from multiple hiPS cell lines.

Western blot. Human cortical spheroids were rapidly lysed on ice with the RIPA lysis buffer system (Santa Cruz, sc-24948) after low-oxygen exposure. Whole-cell lysates were then separated on gels (Invitrogen, NuPAGE 4–12% Bis-Tris) and transferred to a PVDF membrane (Millipore, Immobilon-P Membrane, 0.45 μm). The membranes were incubated at 4°C overnight with the following primary antibodies: HIF-1 α (mouse, 1:1,000, BD Bioscience, 610958)

β -actin (mouse, 1:20,000, Sigma, A5316) and c-CAS3 (rabbit, 1:500, Abcam, ab32042). Horseradish peroxidase-conjugated anti-mouse or anti-rabbit IgG was used as secondary antibody. Signals were developed by chemiluminescence (Amersham, ECL western blotting detection reagents, RPN2106). Bands were quantified using ImageJ software, with normalization to background and to a β -actin control. Uncropped blots of representative western blots are shown in the Source Data and values from quantification for all blots used are listed in Supplementary Table 2.

Real-time quantitative PCR. mRNA was isolated using the RNeasy Mini kit and RNase-Free DNase set (Qiagen), and template cDNA was prepared by reverse transcription using the SuperScript III First-Strand Synthesis SuperMix for qPCR with reverse transcription (Life Technologies). Quantitative PCR was performed using Sybr Green (Roche) on a ViiA7 machine (Applied Biosystems, Life

Technologies). Data were processed using QuantStudio RT-PCR software (Applied Biosystems). Primers and sequences are listed in Supplementary Table 4.

RNA sequencing. mRNA was isolated using the miRNeasy micro Kit and RNase-Free DNase set (Qiagen). Library preparation was conducted by Macrogen (<https://www.macrogenusa.com>) using the TruSeq Stranded Total RNA LT Sample Prep Kit. Samples were then sequenced on the Illumina HiSeq 4000 System using paired-end, 101-bp-long reads to a minimum of 40 million reads per sample. We used STAR v.2.5.2b (ref. ⁴³) to align raw RNA-seq reads to the GRCh37 human genome reference from the Illumina iGenome Project. We generated alignment quality-control metrics with Picard (<https://www.broadinstitute.github.io/picard>). Principal-component analysis of these metrics did not detect outliers. We then used HTSeq⁴⁴ to generate gene-level count data, and kept transcripts with at least one read in more than 50% of the samples. The CQN R package⁴⁵ normalized the remaining 24,878 transcripts for gene length, GC content and sample library size. We further removed genes whose expression value did not change across all samples or with an average normalized expression value less than one (that is, weakly expressed genes). We screened again with principal-component analysis of normalized gene expression but did not detect outliers.

We conducted hierarchical clustering and differential gene expression analysis with normalized gene-expression values. To identify confounding variables, we used a regression model selection approach. We built negative binomial regression models to model expressions of each gene separately. A forward stepwise algorithm selected the best model, defined as the model where the Bayesian information criterion could not be improved by adding additional confounding variables. With this approach, we identified the three most impactful confounding variables: hiPS cell line, percentage of untranslated region bases and percentage of intronic bases. We used edgeR^{46,47} to identify significant genes at each of the three time points (after 24 h or 48 h of <1% O₂ and after 72 h of reoxygenation) and to remove the effects of the three confounding variables. We corrected *P* values for multiple comparisons using the Benjamini–Hochberg method and selected significant genes on the basis of two criteria: FDR ≤ 0.05 and at least 50% increase or decrease in expression between the control and hypoxia conditions (that is, a 1.5-fold change, up or down). As a final quality-control step, we identified genes that were differentially expressed across time in the control samples (that is, highly correlated with time) and removed them from the list of differentially expressed genes. As the fold-change threshold is somewhat arbitrary we list the entire set of genes with FDR ≤ 0.05 in the supplementary material, along with log₂-transformed fold-changes (Supplementary Table 3). We combined all significant genes identified at all three time points to generate a heat map of all samples (heatmap3 R package). We used the GoSeq⁴⁸ R package as well as ToppGene⁴⁹ to identify Gene Ontology (GO) terms enriched in our significant gene list.

To examine the relationship between differential gene expression and the developing human cortex, we used layer-specific data that were previously reported for PCW 21 (ref. ¹⁶). We used a hypergeometric test (two-sided) to assess enrichment, and corrected *P* values for multiple comparisons using the Bonferroni correction. We determined the background for these calculations as the number of genes overlapping between our RNA-seq data and the data reported in Miller et al.¹⁶. To ensure that our choice of a 1.5-fold-change threshold did not affect the results of these analyses, we also conducted exploratory analyses to assess whether the enrichment for SVZ transcripts was robust at different thresholds. We observed that this enrichment was stable across a wide range of fold-change thresholds (approximately 1.3-fold to 2.5-fold-change).

We conducted gene coexpression analysis following normalization for gene length and GC content (using CQN; see above). The WGCNA³⁰ R package

computed an unsigned similarity matrix with a softpower of 12. We created gene modules on the basis of hierarchical clustering results of the similarity matrix and summarized the ‘average’ expression of all the genes in a given module with the first principal component of module expression (module ‘eigengene’). We then evaluated the relationship between these gene modules and experimental conditions (that is, oxygen tension) by computing correlation coefficients to the first principal component. We identified a total of nine significant gene coexpression modules based on two cutoffs: correlation coefficient ≥ 0.9 and FDR ≤ 0.05. We conducted GO enrichment analysis of the genes in each of these nine significant modules with the R package GoSeq⁴⁸. Only two modules were significantly enriched for GO terms after FDR correction: the blue and turquoise modules.

Statistics. Data are presented as mean ± s.e.m., unless otherwise indicated. Distributions of the raw data were tested for normality of distribution; statistical analyses were performed accordingly using paired or unpaired *t*-test (two sided), Mann–Whitney *U* test, Wilcoxon rank-sum test, or the Friedman or ANOVA test with multiple-comparison correction as indicated. Sample sizes were estimated empirically. GraphPad Prism v.7 was used for statistical analyses.

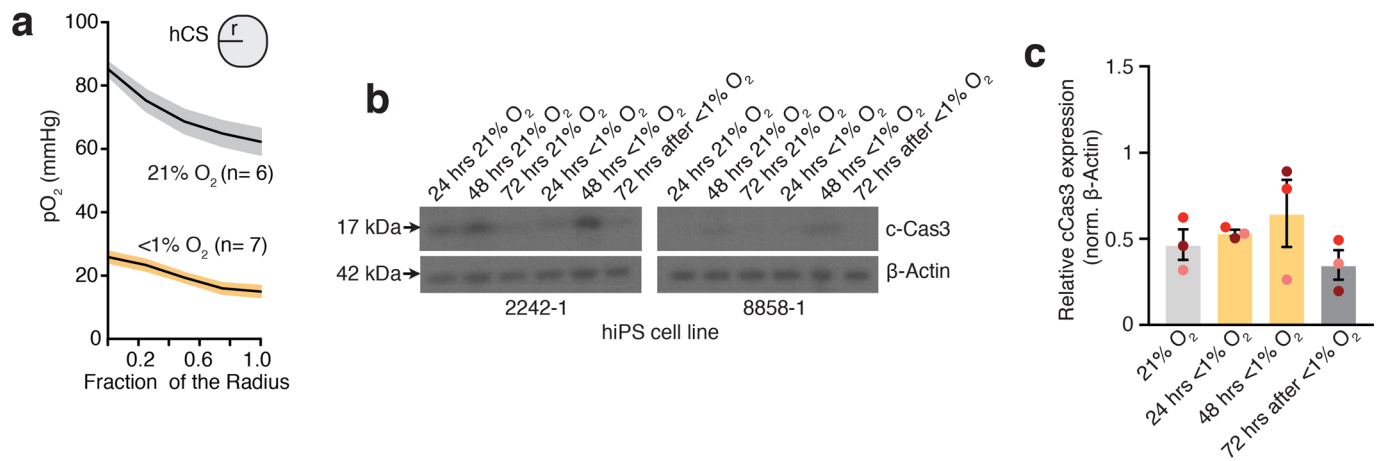
Reporting Summary. Further information on research design is available in the Nature Research Reporting Summary linked to this article.

Data availability

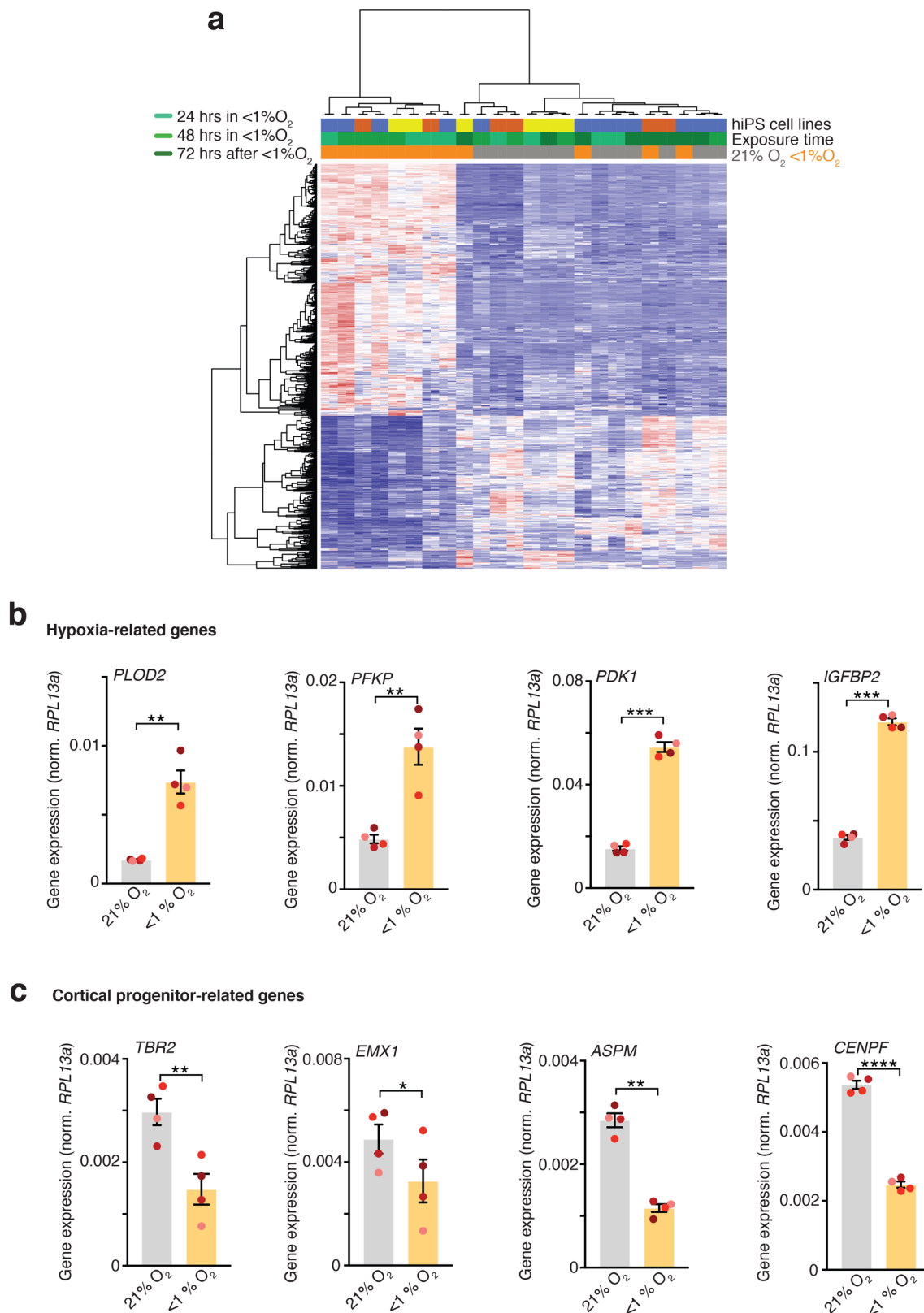
Gene expression data are available in the Gene Expression Omnibus (GEO) under accession number [GSE112137](https://www.ncbi.nlm.nih.gov/geo/query/acc.cgi?acc=GSE112137). The data that support the findings of this study are available on request from the corresponding author.

References

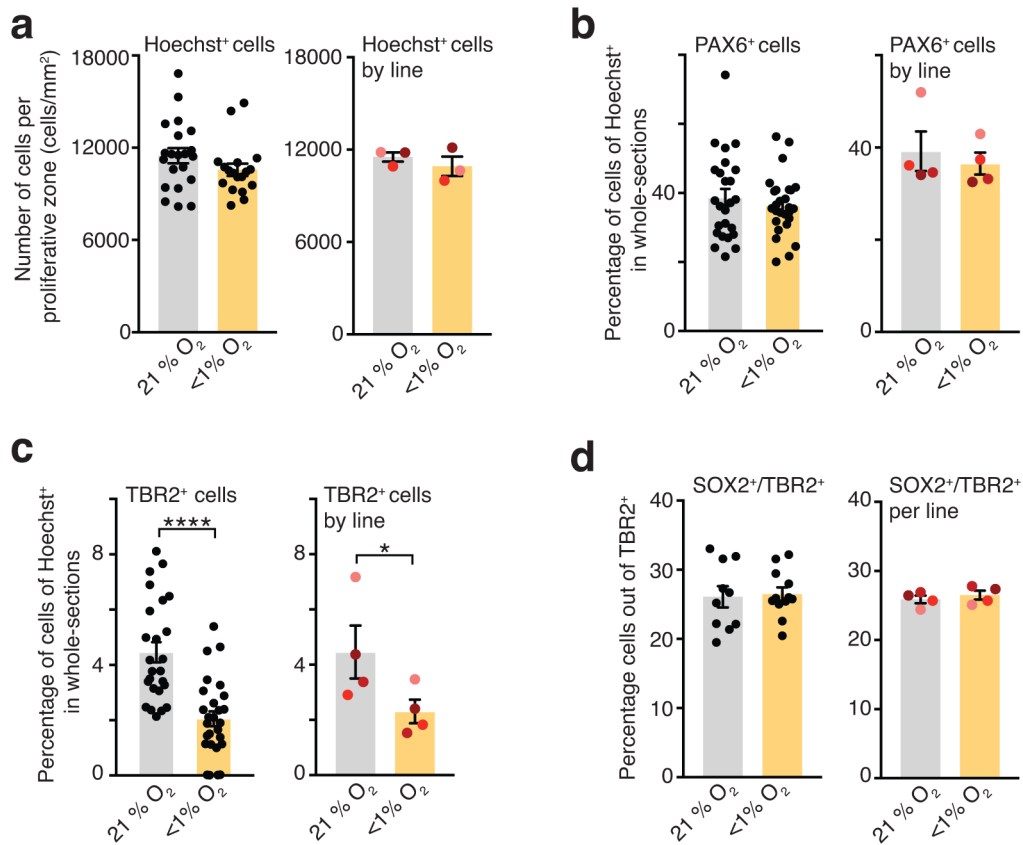
- Paşca, S. P. et al. Using iPSC-derived neurons to uncover cellular phenotypes associated with Timothy syndrome. *Nat. Med.* **17**, 1657–1662 (2011).
- Lui, J. H. et al. Radial glia require PDGFR α –PDGFR β signalling in human but not mouse neocortex. *Nature* **515**, 264–268 (2014).
- Dobin, A. et al. STAR: ultrafast universal RNA-seq aligner. *Bioinformatics* **29**, 15–21 (2013).
- Anders, S., Pyl, P. T. & Huber, W. HTSeq—a Python framework to work with high-throughput sequencing data. *Bioinformatics* **31**, 166–169 (2015).
- Hansen, K. D., Irizarry, R. A. & Wu, Z. Removing technical variability in RNA-seq data using conditional quantile normalization. *Biostatistics* **13**, 204–216 (2012).
- McCarthy, D. J., Chen, Y. & Smyth, G. K. Differential expression analysis of multifactor RNA-seq experiments with respect to biological variation. *Nucleic Acids Res.* **40**, 4288–4297 (2012).
- Robinson, M. D., McCarthy, D. J. & Smyth, G. K. edgeR: a Bioconductor package for differential expression analysis of digital gene expression data. *Bioinformatics* **26**, 139–140 (2010).
- Young, M. D., Wakefield, M. J., Smyth, G. K. & Oshlack, A. Gene ontology analysis for RNA-seq: accounting for selection bias. *Genome Biol.* **11**, R14 (2010).
- Chen, J., Bardes, E. E., Aronow, B. J. & Jegga, A. G. ToppGene Suite for gene list enrichment analysis and candidate gene prioritization. *Nucleic Acids Res.* **37**, W305–W311 (2009).
- Langfelder, P. & Horvath, S. WGCNA: an R package for weighted correlation network analysis. *BMC Bioinformatics* **9**, 559 (2008).



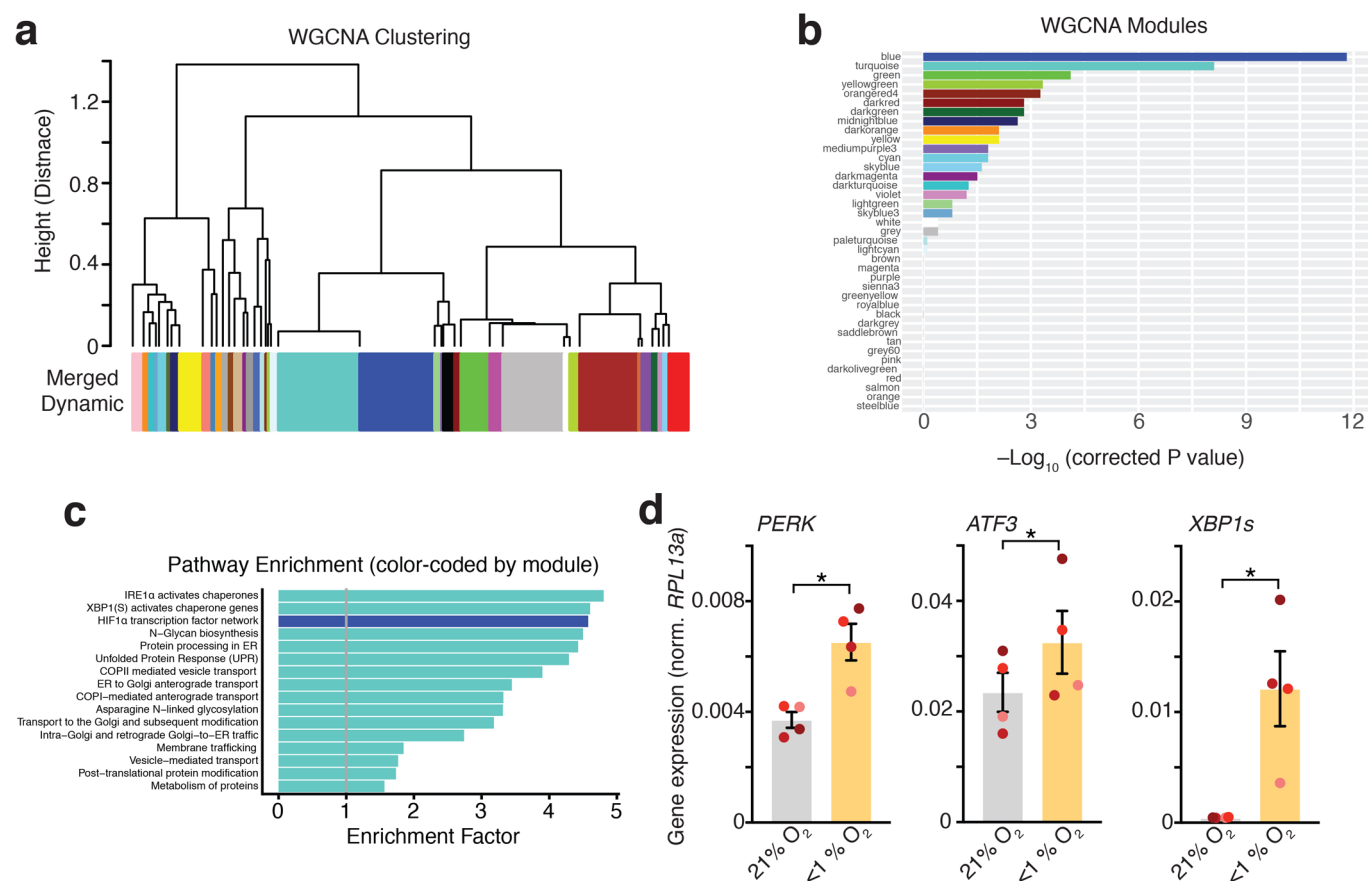
Extended Data Fig 1 | Oxygen tension and c-CAS3 in hCS following hypoxia. **a**, Oxygen tension (P_{O_2} , mm Hg) measurements inside hCS from Fig. 1b, shown as a function of depth (values for each hCS was normalized as a function of its radius) ($n=6$ hCS for 21% O_2 and $n=7$ hCS for <1% O_2); from three hiPS cell lines). Shaded area indicates s.e.m. **b,c**, Representative western blots (**b**) and quantification (**c**) of c-CAS3 in hCS after 24 h and 48 h of exposure to <1% O_2 and at 72 h after reoxygenation (one-way ANOVA, $F_{3,6}=1.56$, $P=0.29$); normalized to β -actin ($n=3$ differentiated hiPS cell lines with two hCS per condition; each line is shown in a different color). Western blots were cropped to show the relevant bands; molecular weight markers are indicated on the left (in kDa). See Supplementary Table 2 for quantifications. Uncropped blots are available as source data. Data are the mean \pm s.e.m. Individual values are indicated by dots.



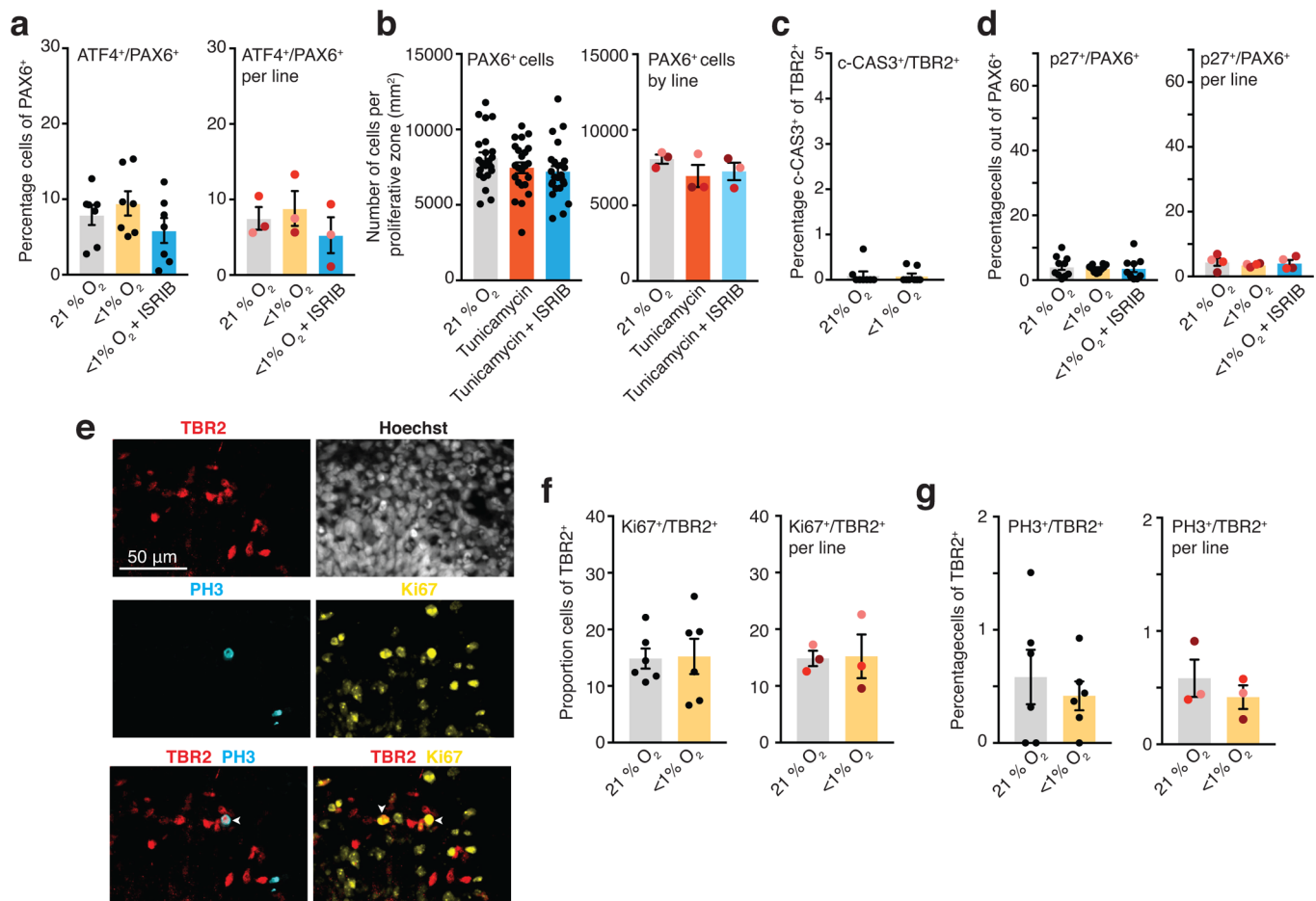
Extended Data Fig 2 | Gene expression changes in hCS following oxygen deprivation. **a**, Hierarchical clustering of RNA-seq data showing clustering of samples on the basis of exposure to oxygen concentration. Samples ($n=24$) from hCS differentiated from three hiPS cell lines were collected after 24 h or 48 h exposure to $<1\%O_2$, as well as 72 h after reoxygenation. We clustered on the basis of all differentially expressed genes identified (1,754 unique genes). Clustering with all expressed genes results in a similar dendrogram (data not shown). **b,c**, Validation by qPCR of hypoxia-related genes *PLOD2* (two-tailed paired t -test, $**P=0.006$), *PFKP* (two-tailed paired t -test, $**P=0.008$), *PDK1* (two-tailed paired t -test, $***P=0.0005$) and *IGFBP2* (two-tailed paired t -test, $***P=0.0002$), and cortical progenitor and cell cycle-related genes *EOMES* (also known as *TBR2*) (two-tailed paired t -test, $**P=0.006$), *EMX1* (two-tailed paired t -test, $*P=0.02$), *ASPM* (two-tailed paired t -test, $**P=0.002$) and *CENPF* (two-tailed paired t -test, $****P<0.0001$), which were identified in the RNA-seq analysis ($n=4$ hiPS cell lines differentiated; each line is shown in a different color; expression normalized to the *RPL13a* housekeeping gene). Data are the mean \pm s.e.m. Individual values are indicated by dots.



Extended Data Fig 3 | Immunocytochemistry quantifications in hCS following oxygen deprivation. **a**, Quantification of the density of Hoechst⁺ cells in proliferative areas in hCS after 48 h exposure to <1% O₂. Data are shown as averages across individual hCS proliferative zones from three hiPS cell lines per condition (left, $n=21$ areas for 21% O₂ versus $n=18$ areas for <1% O₂; two-tailed Mann-Whitney test, $P=0.09$) and as averages across different hiPS cell lines (right, $n=3$ hiPS cell lines, two-tailed Wilcoxon test, $P=0.50$). **b**, Quantification of the percentage of PAX6⁺ cells in whole cryosections of hCS after 48 h exposure to <1% O₂. Data are shown as averages across whole sections of hCS from four hiPS cell lines per condition (left, $n=25$ sections for 21% O₂ versus $n=23$ sections for <1% O₂; two-tailed unpaired t -test, $P=0.44$) or as averages across different hiPS cell lines (right, $n=4$ hiPS cell lines; two-tailed Wilcoxon test, $P=0.25$). **c**, Quantification of the percentage of TBR2⁺ cells in whole cryosections of hCS after 48 h exposure to <1% O₂. Data are shown as averages across whole sections of hCS from four hiPS cell lines per condition (left, $n=25$ sections for 21% O₂ versus $n=27$ sections for <1% O₂; two-tailed Mann-Whitney U test, **** $P<0.0001$) or as averages across different hiPS cell lines (right, $n=4$ hiPS cell lines; two-tailed paired t -test, * $P=0.03$; each line is shown in a different color). **d** Quantification of the percentage of cells coexpressing SOX2 and TBR2 in cryosections of hCS after 48 h exposure to <1% O₂. Data are shown as averages across individual hCS cryosections from four hiPS cell lines per condition (left, $n=10$ sections for 21% O₂ and $n=12$ sections for <1% O₂; two-tailed unpaired t -test, $P=0.82$; from four hiPS cell lines) or as averages across different hiPS cell lines (right, $n=3$ hiPS cell lines; two-tailed paired t -test, $P=0.06$; each line is shown in a different color). Data are the mean \pm s.e.m.; individual values are indicated by dots.



Extended Data Fig 4 | Transcriptome analyses in hCS following oxygen deprivation. **a**, Hierarchical clustering of WGCNA modules identified in the RNA-seq data. Clustering is based on the module eigengenes (average expression profile of all module genes). The turquoise and blue modules are very similar in overall eigengene expression pattern. **b**, Statistical significance for correlation of each module with exposure to low oxygen (bars are labeled by the color of the modules). The blue and turquoise modules are highly associated with exposure (FDR ≤ 0.05). **c**, Enrichment for pathways in the turquoise and blue modules (bars are labeled by the color of the modules in which they are enriched). Only pathways with Bonferroni-corrected FDR $< 1 \times 10^{-4}$ are shown. **d**, Validation by qPCR of the UPR-related genes *PERK* (two-tailed paired *t*-test, $*P = 0.03$), *ATF3* (two-tailed paired *t*-test, $*P = 0.03$) and *XBP1s* (two-tailed paired *t*-test, $*P = 0.04$), which were identified in the RNA-seq analysis ($n = 4$ hiPS cell lines; each line is shown in a different color; expression normalized to the *RPL13a* housekeeping gene). Data are the mean \pm s.e.m.; individual values are indicated by dots.



Extended Data Fig 5 | Quantifications in hCS following oxygen deprivation or tunicamycin exposure. **a**, Quantification of the percentage of cells coexpressing ATF4 and PAX6 in cryosections of hCS after 48 h exposure to <1% O₂ in the presence or absence of 10 nM ISRIB. Data are shown as averages across individual hCS cryosections from three hiPS cell lines per condition (left, $n = 7$ sections for 21% O₂ and $n = 7$ sections for <1% O₂ versus $n = 7$ sections for <1% O₂ + ISRIB; one-way ANOVA $F_{2,18} = 1.37$, $P = 0.27$; Dunnett's multiple-comparison test versus 21% O₂, $P = 0.70$, $P = 0.54$), or as averages across different hiPS cell lines (right, $n = 3$ hiPS cell lines; one-way ANOVA, $F_{2,4} = 4.64$, $P = 0.09$; Dunnett's multiple-comparison test versus 21% O₂, $P = 0.48$, $P = 0.21$; each line is shown in a different color). **b**, Quantification of the density of PAX6⁺ cells in hCS after exposure for 48 h to 1.2 μM tunicamycin in the presence or absence of 10 nM ISRIB. Data are shown as averages across individual hCS proliferative zones from three hiPS cell lines per condition (left, $n = 22$ areas for 21% O₂, $n = 23$ areas for tunicamycin, $n = 24$ areas for tunicamycin + ISRIB; one-way ANOVA, $F_{2,66} = 1.57$, $P = 0.21$; Dunnett's multiple-comparison test versus 21% O₂, $P = 0.37$, $P = 0.15$), or as averages across different hiPS cell lines (right, $n = 3$ hiPS cell lines; Friedman's test, $P = 0.19$; Dunnett's multiple-comparison test versus 21% O₂, $P = 0.20$, $P = 0.08$; each line is shown in a different color). **c**, Percentage of TBR2⁺ cells that coexpress c-CAS3 in whole cryosections of hCS maintained in 21% O₂ or exposed to <1% O₂ for 48 h. (two-tailed Mann-Whitney U test, $P > 0.99$; $n = 8$ cryosections from two hiPS cell lines). **d**, Quantification of the percentage of cells coexpressing p27 and PAX6 in cryosections of hCS after 48 h exposure to <1% O₂ in the presence or absence of 10 nM ISRIB. Data are shown as averages across individual hCS cryosections from four hiPS cell lines per condition (left, $n = 10$ sections for 21% O₂ versus $n = 10$ sections for 1% O₂ and $n = 9$ sections for <1% O₂ + ISRIB; one-way ANOVA, $F_{2,26} = 0.10$, $P = 0.90$ Dunnett's multiple-comparison test versus 21% O₂, $P = 0.88$, $P = 0.90$), or as averages across different hiPS cell lines (right, $n = 4$ hiPS cell lines; one-way ANOVA $F_{2,6} = 0.30$, $P = 0.74$; Dunnett's multiple-comparison test versus 21% O₂, $P = 0.67$, $P = 0.94$; each line is shown in a different color). **e**, Representative images of cells coexpressing TBR2, Ki67 and PH3 in cryosections of hCS. White arrows show examples of cells that are TBR2⁺PH3⁺ or TBR2⁺Ki67⁺. **f**, Quantification of the percentage of cells coexpressing Ki67 and TBR2 in cryosections of hCS after 48 h exposure to <1% O₂. Data are shown as averages across individual hCS cryosections from three hiPS cell lines per condition (left, $n = 6$ sections for 21% O₂ versus $n = 6$ sections for <1% O₂; two-tailed unpaired t -test, $P = 0.91$) or as averages across different hiPS cell lines ($n = 3$ hiPS cell lines; two-tailed paired t -test, $P = 0.91$; each line is shown in a different color). **g**, Quantification of the percentage of cells coexpressing PH3 and TBR2 in cryosections of hCS after 48 h exposure to <1% O₂. Data are shown as averages across individual hCS cryosections from three hiPS cell lines per condition ($n = 6$ sections for 21% O₂ versus $n = 6$ sections for <1% O₂; two-tailed unpaired t -test, $P = 0.55$) or as averages across different hiPS cell lines (right, $n = 3$ hiPS cell lines; two-tailed paired t -test, $P = 0.56$; each line is shown in a different color). Data are the mean \pm s.e.m.; individual values are indicated by dots.

Reporting Summary

Nature Research wishes to improve the reproducibility of the work that we publish. This form provides structure for consistency and transparency in reporting. For further information on Nature Research policies, see [Authors & Referees](#) and the [Editorial Policy Checklist](#).

Statistical parameters

When statistical analyses are reported, confirm that the following items are present in the relevant location (e.g. figure legend, table legend, main text, or Methods section).

n/a Confirmed

- The exact sample size (n) for each experimental group/condition, given as a discrete number and unit of measurement
- An indication of whether measurements were taken from distinct samples or whether the same sample was measured repeatedly
- The statistical test(s) used AND whether they are one- or two-sided
Only common tests should be described solely by name; describe more complex techniques in the Methods section.
- A description of all covariates tested
- A description of any assumptions or corrections, such as tests of normality and adjustment for multiple comparisons
- A full description of the statistics including central tendency (e.g. means) or other basic estimates (e.g. regression coefficient) AND variation (e.g. standard deviation) or associated estimates of uncertainty (e.g. confidence intervals)
- For null hypothesis testing, the test statistic (e.g. F , t , r) with confidence intervals, effect sizes, degrees of freedom and P value noted
Give P values as exact values whenever suitable.
- For Bayesian analysis, information on the choice of priors and Markov chain Monte Carlo settings
- For hierarchical and complex designs, identification of the appropriate level for tests and full reporting of outcomes
- Estimates of effect sizes (e.g. Cohen's d , Pearson's r), indicating how they were calculated
- Clearly defined error bars
State explicitly what error bars represent (e.g. SD, SE, CI)

Our web collection on [statistics for biologists](#) may be useful.

Software and code

Policy information about [availability of computer code](#)

Data collection

Image J (Fiji), Zeiss M1 AxioScope, Keyence BZ-X710.

Data analysis

GraphPad Prism v7. QuantStudio RT-PCR v1.1. For RNAseq: R version 3.3.2, WGCNA v1.61, Goseq v1.26.0, Cqn v1.24.0, heatmap3 v1.1.1, edgeR v3.16.5, bedtools v2.25.0, HTSeq v0.9.1, ToppGene (March 2018 version), picard v2.1.1. Code available at <https://bitbucket.org/willseylab/human-cellular-model-of-hypoxic-brain-injury-of-prematurity>.

For manuscripts utilizing custom algorithms or software that are central to the research but not yet described in published literature, software must be made available to editors/reviewers upon request. We strongly encourage code deposition in a community repository (e.g. GitHub). See the Nature Research [guidelines for submitting code & software](#) for further information.

Data

Policy information about [availability of data](#)

All manuscripts must include a [data availability statement](#). This statement should provide the following information, where applicable:

- Accession codes, unique identifiers, or web links for publicly available datasets
- A list of figures that have associated raw data
- A description of any restrictions on data availability

GSE112137

Field-specific reporting

Please select the best fit for your research. If you are not sure, read the appropriate sections before making your selection.

Life sciences Behavioural & social sciences

For a reference copy of the document with all sections, see [nature.com/authors/policies/ReportingSummary-flat.pdf](https://www.nature.com/authors/policies/ReportingSummary-flat.pdf)

Life sciences

Study design

All studies must disclose on these points even when the disclosure is negative.

Sample size	Sample sizes estimated empirically, based on previous studies in the field.
Data exclusions	No data were excluded from analyses.
Replication	Experiments were performed using 5 individual hiPS cell lines derived from 4 healthy subjects. For each type of experiment we collected multiple hCS from each differentiation. Data for every type of experiment was collected from up to 6 individual differentiations of each hiPS cell line. All replicates for each type of experiment are indicated in the manuscript and in Supplementary Table 1.
Randomization	hCS of similar diameter were randomly selected for each type of experiment.
Blinding	The investigators were not blind to the hypoxia experimental conditions.

Materials & experimental systems

Policy information about [availability of materials](#)

n/a	Involvement in the study
<input checked="" type="checkbox"/>	<input type="checkbox"/> Unique materials
<input type="checkbox"/>	<input checked="" type="checkbox"/> Antibodies
<input type="checkbox"/>	<input checked="" type="checkbox"/> Eukaryotic cell lines
<input checked="" type="checkbox"/>	<input type="checkbox"/> Research animals
<input checked="" type="checkbox"/>	<input type="checkbox"/> Human research participants

Antibodies

Antibodies used	<p>ICC:</p> <p>Rat anti-CTIP2 (Abcam, AB18465), used 1:300 Rabbit anti-cCas3 (Asp175) (CST, #9661, Lot. 45) used 1:400 Rabbit anti-SOX2 (CST, #3579, Lot. 5). used 1:200 Mouse anti-TBR2 (R&D, MAB6166), used 1:100 - hCS Sheep anti-TBR2 (Novus Biologicals, AF6166), used 1:100 - HFT Rabbit anti-PAX6 (Biolegend, PRB-278P), used 1:300 Rabbit anti-p27 (Thermo Fisher Scientific, PA5-27188), used 1:100 Rabbit anti-ATF4 (Cell Signaling, D4B8, 11815), used 1:50 Mouse anti-HIF-1α (Santa Cruz, sc-53546), used 1:50 Rat anti-PH3 (Abcam, AB10543), used 1:500 Rabbit anti-Ki67 (Novus Biological, NB600-1252), used 1:100</p> <p>WB:</p> <p>Mouse anti-HIF-1α (BD bioscience, 610958), used 1:1000 Mouse anti-β-actin (Sigma, A5316), used 1:20,000 Rabbit anti-cCas3 (Abcam, ab32042), used 1:500</p>
Validation	<p>All antibodies were commercially available. We used or validated some of the antibodies in previous studies (Pasca et al., Nature Methods 2015; Sloan et al., Neuron 2017; Birey et al., Nature 2017; Sloan et al., Nature Protocols, 2018; Yoon et al., Nature Methods, 2019), e.g., CTIP2, SOX2, TBR2, PAX6, PH3 (in human cells).</p> <p>ICC:</p> <p>The rat anti-CTIP2 (Abcam, AB18465) has been used in 293 studies according manufacturer's website, and tested for immunofluorescence staining in human fetal brains (Ozai et al., 2018).</p> <p>The rabbit anti-cCas3 (CST, #9661) has been used in 3319 studies according manufacturer's website, and also tested for</p>

immunocytochemistry in human cells (Imaizumi et al., 2018).

The rabbit anti-SOX2 (CST, #3579) has been used in 112 studies according manufacturer's website, and tested for immunofluorescence staining in human cells (Kogut et al., 2018).

The mouse anti-TBR2 (R&D, MAB6166) has been used in 1 study according manufacturer's website.

The sheep anti-TBR2 (Novus Biologicals, AF6166) has been used in 1 study according manufacturer's website.

The rabbit anti-PAX6 (Biolegend, PRB-278P) has been used in 60 studies according manufacturer's website, and tested for immunofluorescence staining in human cells (Chaudhari et al., 2017).

The rabbit anti-p27 (Thermo Fisher Scientific, PA5-27188) has been used in 2 studies according manufacturer's website.

The rabbit anti-ATF4 (Cell Signaling, D4B8, 11815) has been used in 140 studies according manufacturer's website.

The mouse anti- HIF-1 α (Santa Cruz, sc-53546) has been used in 114 studies according manufacturer's website, and tested for immunofluorescence staining in human cells (Nalwoga et al., 2016).

The rat anti- PH3 (Abcam, AB10543) has been used in 39 studies according manufacturer's website, and tested for immunofluorescence staining in human cells (Bershteyn et al, 2017).

The rabbit anti-Ki67 (Novus Biological, NB600-1252) has been used in 37 studies according manufacturer's website, and tested for immunofluorescence staining in human cells (Burks et al, 2018).

WB:

The mouse anti- HIF-1 α (BD Biosciences, 610958) has been used in 201 studies according manufacturer's website, and tested for western blot analysis in human cells (Koeppen et al., 2018).

The mouse anti- β -actin (Sigma, A5316) has been used in 1670 studies according manufacturer's website, and tested for western blot analysis in human cells (Gabriel-Salazar et al., 2018).

The rabbit anti-cCas3 (Abcam, ab32042) has been used in 89 studies according manufacturer's website, and tested for western blot analysis in human cells (Zhao et al., 2017).

Eukaryotic cell lines

Policy information about [cell lines](#)

Cell line source(s)

hiPS cell lines from were derived at Stanford University with IRB approval and written consent. Inactivated mouse fibroblasts EmbryoMax PMEF were purchased from EMD Millipore.

Authentication

All hiPS cell lines were assessed for pluripotency and genomic integrity (by Cyto-SNP arrays).

Mycoplasma contamination

All cell lines and PMEF were tested for Mycoplasma contamination and tested negative

Commonly misidentified lines
(See [ICLAC](#) register)

No commonly misidentified cell lines were used.

Method-specific reporting

n/a	Involvement in the study
<input checked="" type="checkbox"/>	<input type="checkbox"/> ChIP-seq
<input checked="" type="checkbox"/>	<input type="checkbox"/> Flow cytometry
<input checked="" type="checkbox"/>	<input type="checkbox"/> Magnetic resonance imaging